MLM-1179
TID-4500 (26th Ed.)
Category - UC-2
Progress Reports

# MOUND LABORATORY PROGRESS REPORT FOR DECEMBER, 1963

J. F. Eichelberger
G. R. Grove
L. V. Jones

**Date:** December 31, 1963

The Mound Laboratory Progress Report, issued monthly, is intended to be a means of reporting items of current technical interest in research and development programs. To issue this report as soon as possible after the end of the month, editorial work is limited; and since this is an informal progress report, the results and data presented are preliminary and subject to change.

These reports are not intended to constitute publication in any sense of the word. Final results either will be submitted for publication in regular professional journals or will be published in the form of MLM topical reports.

The previous reports in this series are:

MLM-1178
MLM-1177
MLM-1176
MLM-1175
MLM-1170
MLM-1160

**MONSANTO RESEARCH CORPORATION**

A SUBSIDIARY OF MONSANTO CHEMICAL COMPANY

**MOUND LABORATORY**

MIAMISBURG, OHIO OPERATED FOR

**UNITED STATES ATOMIC ENERGY COMMISSION**

U.S. GOVERNMENT CONTRACT NO. AT-33-1-GEN-53

# TABLE OF CONTENTS

## DISCLAIMER

# SUMMARY

## Adhesives and Plastics Research

*Adhesives* Two polysulfide-based conductive adhesives were prepared and evaluated. One formulation, cured with an amine, increased in resistivity (from 0.30 to 50 ohm-cm) when heated at 160°F. The second, cured with lead oxide, retained its low resistivity (from 0.12 to 0.15 ohm-cm) on heating. This latter material had an adequate tensile bond strength (350 psi), but it had a lower than optimum peel strength.

*Plastics* Zirconia fibers were evaluated as a filler for diallyl phthalate molding powders. Tensile strength, impact strength, and heat distortion temperatures were similar for zirconia and asbestos-filled plastics. The arc resistance values of the zirconia-filled formulations were lower than those of the asbestos-filled material. There appears to be no advantage in substituting zirconia fibers for asbestos in the diallyl phthalate molding powders.

## Radioelements

*Polonium-209 Half-life* A half-life value of 40.2 ± 2.6 years for polonium-209 was determined by measuring the total polonium by absorption spectrophotometry and the total alpha activity indirectly by gamma counting.

*Polonium Decay Scheme Studies* A recent determination of the alpha decay energy of astatine-212 allows the calculation of the energy available for electron capture ($Q_{EC}$) of polonium-208. The estimate of $Q_{EC}$ for polonium-208 indicates that a level in bismuth-208 at 1.43 Mev may be populated in the decay of polonium-208.

A detailed study of the decay properties of a source of mixed polonium-208 and polonium-209 is in progress. Triple gamma coincidence spectrum measurements have led to the tentative identification of a peak in the range of 860 to 900 kev as a cross-over state in polonium-208. Energy assignments are difficult because of a counting rate of 0.16 count per minute per channel at the peak.

*Determination of Coincidence Correction* The half-life of lead-211 was computed from 28 sets of data with two different expressions for the resolving time of the proportional counter. There was good agreement between the grand means obtained by the two methods, but the individual half-life values were externally inconsistent. It was found that neither expression adequately described the dead-time losses at counting rates above $10^6$ counts per minute.

*Half-life of Radium-223* The half-life of radium-223 was recomputed with counting rate limits lower than those previously applied, and the agreement between the calorimetric and alpha-counting results was improved. The radium-223 half-life may be useful in determining the resolving time corrections to be used in the proportional counter.

*Residue Adsorption* Purification of the barium-140 stock solution was completed, and the interfering impurity was identified as calcium. Reversal of the usual order of adsorption of barium and lanthanum was found to occur when the adsorbed material was leached with sulfuric acid.

## Isotope Separation

*Helium-3* The Weber-Schmidt Equation was used to obtain predicted thermomolecular pressure corrections on saturated vapor as a function of temperature for a number of pressure sensing tube diameters used with the helium-3 thermometer.

Recent difficulties in obtaining satisfactory counting plateaus on gas-filled Geiger tubes were corrected. Attempts to obtain normal plateaus by increasing the isobutane content in the counting gas were unsuccessful. An additional resistor and capacitor used to modify the G.M. input circuit of the scaler decreased the pulse to the scaling circuit to an acceptable size.

*Equation of Continuity for the Cylindrical Case.* The longitudinal concentration profile in a thermal diffusion column was determined using the Equation of Continuity to obtain the partial differential equation of flow in the column. Then the radial and axial portions of the partial differential equation were uncoupled. The justification for this uncoupling is that radial concentration differences are extremely small compared to the total separation in the column. The radial effect was treated as a perturbation, and the solution was arranged so that the primary terms were similar to those of the Jones and Furry theory. Succeedingly smaller correction terms may be applied to the main terms. The solution, of necessity numerical in nature, was obtained by additional numerical integrations of the terms of the operation.

*Carbon-13* The preparation of gram quantities of greater than 90 per cent purity carbon-13 is a major activity. Transport studies are being made of carbon monoxide and methane for feed evaluation. The eight-stage cascade system was converted to a nine-stage cascade system of eleven hot-wire and concentric-tube columns. The nine-stage system enriched natural methane to 97.9 per cent mass-17 in 53.7 per cent methane. Eight and a half grams of over 90 per cent carbon-13 product have been accumulated containing about 10 per cent impurities. Chemical exchange and distillation are being studied for enrichment and purification of feed material for the thermal column system.

Complete thermal diffusion column transport data have been obtained for carbon monoxide at a wire temperature of 500°C, and column transport coefficients have been computed.

A method was developed to select the optimum boilup for any given carbon-13 production rate, i.e., the production rate which results in a minimum length column for the given separation. The three factors used to select the optimum conditions were: (1) actual theoretical stage requirement; (2) height equivalent to one theoretical stage; and (3) average relative volatility.

*Neon* Studies were made using two neon thermal diffusion columns in a two-stage cascade to separate a binary mixture of neon-20 and neon-21. A determination was made of the flow rate and the length of time during which greater than 99 per cent neon-20 could be drawn off.

*Krypton* A two-column, hot-wire, thermal diffusion cascaded unit with an infinite reservoir at the bottom processed natural krypton in the first step toward obtaining a final enrichment of over 90 per cent krypton-78 and -80. Twenty-four liters of krypton containing about nine per cent krypton-78 and -80 were obtained.

A sample of 0.4 per cent krypton-85 will be enriched for use in a calorimetric half-life determination. A sample capsule has been designed for the krypton-85, which will be enriched by chromatography.

## Alpha and Neutron Source Development

*Neutron Sources* Measurements were made to determine the effect of changes in temperature of the precision long counter (PLC) on the measured counting rates for neutron sources. For the internal standard source a counting rate decrease of 0.034 per cent occurred with a temperature increase of one degree Centigrade. The fluctuation of the counting rate with temperature may be explained by assuming that the source moves perpendicularly to the axis of the $BF_3$ counter; the counting rate is proportional to the inverse square of the distance of the source from the counter; therefore, the counting rate decreases with temperature increase. Results obtained with an external source were inconclusive.

One new PuBe source was shipped and four recanned sources were returned to their users.

## Analytical

*Calorimetry* The most precise and accurate calorimetric determinations are currently made by comparing the bridge unbalances of a sample and a calibrating heater using a recorder; in this type of determination all but 25 to 100 microvolts are suppressed by resistance shunting one of the sample arms of the bridge. This system has three main advantages: (1) the constancy of the bridge current is less critical than in the sampling technique with a potentiometer-galvanometer system; (2) no error results from the decade box (used for the shunt resistance); and (3) any thermal emf developed in the shunt circuit is reduced by the ratio of shunt resistance to initial bridge resistance. The sensitivity for this method was plotted as function of power from the calibrating heater; the resultant straight line sloped downward slightly with increasing power. A sensitivity correction was also determined for the effect of the shunting resistance.

*Beryllium by Gamma Activation Analysis* The irradiation and counting systems used in the gamma activation analysis of beryllium have been modified to incorporate four helium-3 filled neutron counting tubes in place of the indium foil formerly used as a detector. The helium-3 neutron detectors have already been used successfully for over a month. Beryllium samples are now neutron counted during the gamma irradiation, as the helium-3 tubes completely discriminate against the high strength gamma field of the antimony-124 source. The neutron tubes have increased the counting efficiency by a factor of 500 compared to the indium foil previously used. Therefore, a 0.05-curie source is used instead of the original three curies, making the analysis less hazardous while maintaining the high neutron count rate necessary for rapid and accurate analyses. This method has a precision of ± 0.2 per cent, and the analysis time is 45 minutes.

*Adhesive formulations are being developed for specialized applications. The cured formulation must be flexible at low temperatures, and it must retain its tensile strength at high temperatures. In addition, the properties of diallyl phthalate formulations are being evaluated to help produce superior plastic parts.*

## Adhesives

Two polysulfide-based conductive adhesives were prepared to check the performance of amine-cured and of lead oxide-cured formulations. The composition and properties of the adhesives are shown in Table 1. These data confirm the findings that amine-cured polysulfide adhesives increase in resistance when heated at 160°F for 24 hours and that the lead oxide-cured materials maintain their low resistivity under these conditions. Formulation CS-20 had a tensile bond strength of 350 psi and a peel strength of 6.5 pounds per inch. This peel strength was lower than desired (20 pounds per inch), but it was higher than that obtained with a comparable polyurethane-based formulation (two pounds per inch).

## Plastics

Zirconia fibers were mixed with diallyl phthalate molding powders to determine whether the resultant formulation would possess characteristics superior to the asbestos-filled plastic now in use. The following formulation was used:

| | Parts |
|---|---|
| Diallyl phthalate prepolymer | 100 |
| Zirconia fibers | 100 |
| Calcium stearate | 2 |
| Tertiary butyl perbenzoate | 2 |
| Hydroquinone | 0.03 |
| Acetone | 15 |

The dry ingredients were mixed directly on the mill rolls, and acetone was added to insure intimate mixing. Test specimens were prepared from the molding powders, and the data were compared with average values obtained for asbestos float filled plastic prepared in the production facility.

Tensile strength, impact strength, and heat distortion temperature values were approximately equal for the zirconia and asbestos-filled plastics; but the arc resistance values of all the zirconia-filled materials were substantially lower (48.3-71.2 seconds) than that of the asbestos-filled material (130 seconds). There appears to be no advantage in substituting zirconia fibers for asbestos filler in the diallyl phthalate molding powders.

Table 1

## COMPOSITION AND PROPERTIES OF CONDUCTIVE POLYSULFIDE ADHESIVES

| Component | Component in Formulation | |
|---|---|---|
| | CS-20[a] | CS-21[a] |
| LP-3 polysulfide polymer[b] | 3.1 | - - |
| LP-8 polysulfide polymer[b] | - - | 10.6 |
| LP-32 polysulfide polymer[b] | 12.4 | - - |
| D. E. R. 332 epoxy resin[c] | - - | 8.5 |
| Butyl glycidyl ether | - - | 2.1 |
| 2,4,6-Tri (dimethylaminomethyl)phenol[d] | - - | 1.1 |
| C5, lead peroxide paste[b] | 2.3 | - - |
| Toluene | 2.9 | - - |
| Continex C. F. Carbon black[e] | 3.1 | 6.7 |
| J-2 Silver Filler[f] | 76.2 | 71.0 |
| | 100 | 100 |
| **Characteristics** | | |
| Working Pot life at R. T. (hr) | 3/4 | 2 |
| Cure Schedule | 16 hr. at 160°F | 24 hr. at R. T. |
| Specific Resistivity (ohm-cm) Before Heat Conditioning | 0.12 | 0.30 |
| Specific Resistivity (ohm-cm) After Heating at 160°F for 24 hours | 0.15 | 50 |
| Tensile Bond Strength (psi) | 350 | 800 |
| Peel Strength (lbs/in.) | 6.5 | Not Determined |

[a]Mound Laboratory Designation.

[b]Thiokol Chemical Co.

[c]Dow Chemical Co.

[d]Rohm and Haas Co.

[e]Witco Chemical Corp.

[f]Engelhard Industries

*Basic and applied research on a number of radioelements is being conducted to determine the physical properties, develop analytical techniques, and study the basic radiochemistry involved. Of particular interest are alpha emitters, their decay chains, their isotopes, and their chemical homologs.*

## Polonium-209 Half-Life

The half-life of polonium-209 was determined in an experiment in which total polonium content of a solution was measured spectrophotometrically, and total alpha activity was measured indirectly by gamma counting small aliquot samples of the solution. (See MLM-1178 for a discussion of experimental details.) Samples of purified polonium metal were dissolved in one drop of 1.5 molar hydrochloric acid, to which one drop of 30 per cent hydrogen peroxide was added. The solutions were boiled to remove peroxide, then carefully diluted in volumetric flasks to 5.00 ± 0.03 ml. The solutions were transferred to the spectrophotometer cells, and two 10-microliter aliquots were removed for gamma counting. Spectrophotometer measurements were made in matched optical cells using a Coleman Model 14 Universal Spectrophotometer.

The experimental results are given in Table 2. The largest source of error is in the determination of the polonium concentration. Hunt[1] gave the Molar Absorbancy Index for polonium-210 in 1.5 molar hydrochloric acid as $(1.06 \pm 0.03) \times 10^4$. The error given in the individual polonium-209 half-life values is based only on the error in the absorbancy index. The average polonium-209 half-life is then 40.2 ± 2.6 years.

**Table 2**

**EXPERIMENTAL RESULTS OF POLONIUM-209 HALF-LIFE DETERMINATION**

| Measurement | Sample 316033-1 | Sample 316056-1 | Sample 316068-1 |
|---|---|---|---|
| Optical density (425 mμ) | 0.324 | 0.490 | 0.380 |
| Po(IV) concentration (M) | $2.351 \times 10^{-5}$ | $3.556 \times 10^{-5}$ | $2.758 \times 10^{-5}$ |
| Total Po weight (g) | $24.51 \times 10^{-6}$ | $37.07 \times 10^{-6}$ | $28.75 \times 10^{-6}$ |
| Total alpha activity (d/m) | $1.825 \times 10^{10}$ | $2.971 \times 10^{10}$ | $2.245 \times 10^{10}$ |
| $Po^{209}$ alpha activity (d/m) | $9.902 \times 10^{8}$ | $1.613 \times 10^{9}$ | $1.218 \times 10^{9}$ |
| $Po^{208}$ alpha activity (d/m) | $1.726 \times 10^{10}$ | $2.810 \times 10^{10}$ | $2.123 \times 10^{10}$ |
| $Po^{208}$ weight (g)[a] | $13.06 \times 10^{-6}$ | $21.26 \times 10^{-6}$ | $16.06 \times 10^{-6}$ |
| $Po^{209}$ weight (g) | $11.45 \times 10^{-6}$ | $15.81 \times 10^{-6}$ | $12.69 \times 10^{-6}$ |
| $Po^{209}$ half life (yrs) | 43.9 ± 2.7 | 37.2 ± 2.5 | 39.6 ± 2.5 |

[a]The $Po^{208}$ half-life was taken to be 1055 days.

An independent determination of the polonium-209 half-life is expected from mass-spectrometer data. In a mass spectrometer experiment performed using tellurium as a substitute for polonium, mass peaks attributable to $Te_2^+$ were observed. The appearance of $Te_2^+$ mass peaks is expected in view of the diatomic nature of tellurium vapor. Polonium is also diatomic in the vapor phase. This means that the polonium mass peaks should occur in the mass range 416 to 418, where no interference from background contamination should occur.

[1]D. J. Hunt, *Absorption Studies of Polonium Complexes in Chloride Solutions*, MLM-979, 1954.

## Polonium Decay Scheme Studies

In a recent paper the decay of astatine-212, which alpha decays to bismuth-208, was described.[2] Jones gives the ground state-ground state alpha particle energy as 7.66 Mev. It is now possible to calculate the energy available (the Q value) for the electron capture decay of polonium-208, using the method of closed cycles. The closed cycle in this case is:

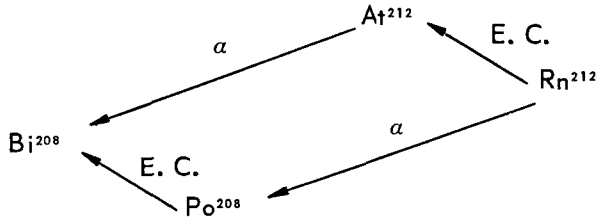


The $Q$ value for the electron capture decay of radon-212 is not well known. It has been estimated to be 0.00 Mev.[3] The value $Q_\alpha$ for astatine-212, using the Jones data, is 7.807 Mev, and $Q_\alpha$ for radon-212, is 6.384 Mev. This leads directly to $Q_{EC}$ of 1.423 Mev for polonium-208.

Since $Q_{EC}$ of polonium-208 is heavily dependent on $Q_{EC}$ of radon-212, the masses of astatine-212 and radon-212 were computed from other nuclear data. The radon-212 mass can be calculated directly from the mass of stable lead-204, and the alpha decay energies of polonium-208 and radon-212, in the following decay sequence:

$$Rn^{212} \xrightarrow{Q_\alpha} Po^{208} \xrightarrow{Q_\alpha} Pb^{204} \text{ (stable)}$$

The atomic mass of radon-212 is 212.05706 atomic mass units (amu) on the physical scale.

The mass of astatine-212 may be computed from the data for the decay chain:

$$At^{212} \xrightarrow{Q_\alpha} Bi^{208} \xrightarrow{Q_{EC}} Pb^{208} \text{ (stable)}$$

However, the value of $Q_{EC}$ for bismuth-208 must also be estimated. Three estimated values of $Q_{EC}$ were obtained: 2.9 Mev,[4] 2.670 Mev,[5] and 2.876 Mev.[6] These $Q_{EC}$ values for bismuth-208 lead to three masses for astatine-212:

| | |
|---|---|
| 212.05701 amu | (Strominger et al.) |
| 212.05676 amu | (Cameron) |
| 212.05699 amu | (Konig et al.) |

[2] W. B. Jones, *Phys. Rev.*, **130**, 2042 (1963).

[3] D. Strominger, J. M. Hollander, and G. T. Seaborg, *Revs. Modern Phys.*, **30**, 585 (1958).

[4] *Ibid.*

[5] A. G. W. Cameron, *A Revised Semi-empirical Mass Formula*, Canada, CRP-690, 1957.

[6] L. A. Konig, J. H. E. Mattouch, and A. H. Wapstra, *Nucl. Phys.*, **31**, 1 (1962).

The three values for the mass of astatine-212 lead to three different values of $Q_{EC}$ for radon-212, and in turn, to three different values for $Q_{EC}$ of polonium-208:

| | |
|---|---|
| 1.467 Mev | (Strominger et al.) |
| 1.697 Mev | (Cameron) |
| 1.490 Mev | (Konig et al.) |

All the estimates of $Q_{EC}$ for bismuth-208 give $Q_{EC}$ for polonium-208 a value greater than 1.43 Mev. This means that the predicted level in bismuth-208 at 1.43 Mev may be populated in the electron capture decay of polonium-208. Previous calculations, based on an estimate of $Q_{\alpha}$ for astatine-212 were ambiguous: values above and below 1.43 Mev for $Q_{EC}$ of polonium-208 were obtained.[7] No evidence for the decay of polonium-208 to this level in bismuth-208 has been obtained in gamma-ray coincidence experiments conducted at Mound Laboratory thus far. Further work is in progress.

Previous coincidence measurements are being analyzed in detail. A triple coincidence spectrum was noted between two detectors gated in the range 50-90 kev and a third detector covering a wide energy range with observable peaks in this coincidence spectrum at energies of 295, 565, and 860-900 kev.[8] It was thought that this latter peak (860-900 kev) was due to random coincidences in polonium-209 decay. However, a careful analysis of these data and single spectra of the various polonium-208-polonium-209 mixtures under study now indicates that this peak is a cross-over state in polonium-208 decay. Assignment of an energy is difficult since only 60 counts per channel were obtained for a 3780-minute measurement.

**Determination of Coincidence Correction**

In a continuing effort to obtain a precise and externally consistent value for the half-life of lead-211, 28 sets of data have been treated by the variational method previously described.[9]

Two solutions were found for each set; the first solution was based on the Ruark and Brammer Equation,[10] which assumes an average time distribution for successive disintegrations, and the second solution was based on the Volz Equation,[11] which describes the dead-time losses by a Poisson time distribution function:

$$\tau_1 = \frac{1}{n} - \frac{1}{N} \qquad \textit{(Ruark and Brammer)}$$

$$\tau_2 = \frac{1}{N} \log_e \left(\frac{N}{n}\right) \qquad \textit{(Volz)}$$

The weighted grand means of the computed half-life values were 35.984 ± 0.034 (from $\tau_1$) and 36.011 ± 0.029 minutes (from $\tau_2$). When Chauvenet's rejection criterion was applied to the individual half-life values (but not to the data from which they were computed), the grand means became 36.000 ± 0.013 and 36.010 ± 0.015 minutes, respectively. Five values were rejected for $\tau_1$ and three for $\tau_2$.

[7]MLM-1160.
[8]MLM-1178.
[9]MLM-1175.
[10]A. E. Ruark, and F. E. Brammer, *Phys. Rev.* **52**, 322 (1937).
[11]H. Volz, *Z. Physik* **93**, 539 (1935).

In spite of the excellent agreement between the two grand means, examination of the individual deviations showed that the data were still externally inconsistent by Birge's criterion,[12] according to which, the ratio of the external probable error to the internal probable error is normally distributed about the mean value, unity, with the modulus of precision $\sqrt{n}$. By this criterion, if the value,

$$hx = \sqrt{n}\left(\frac{P_{ext.}}{P_{int.}} - 1\right)$$

is greater than 1.83, the probability of occurrence is less than 0.01, and the means are considered inconsistent. For the two grand means calculated, the values of $hx$ were 26.75 and 33.49, respectively, even after application of Chauvenet's criterion.

Three sets of data were selected for more detailed examination. Application of Chauvenet's criterion to the individual data revealed that, regardless of which expression was used for the resolving time, every point in excess of a counting rate of $10^6$ counts per minute was rejected. This was true even when an auxiliary scaler was used in place of the mechanical register or when a one-megacycle transistorized scaler was used in place of the slower vacuum tube scaler normally used with the proportional counter.

It is evident, therefore, that neither of the two expressions thus far tested adequately describes the counting losses due to the resolving time of the proportional counter used in these experiments. Future work will be directed towards determining an empirical expression based on an externally consistent value for the half-life of lead-211.

**Half-Life of Radium-223**

The results of a determination of the half-life of radium-223 were reported earlier this year.[13] The computations were made by the "decaying pair" method which, while it requires no knowledge of the value of the resolving time of the proportional counter used, assumes that the dead time losses are described by the Ruark and Brammer Equation of the preceding section (See *Determination of Coincidence Correction*).

In view of the results reported above with respect to the half-life of lead-211, it was thought worthwhile to recalculate the half-life of radium-223 for counting rate limits of $10^6$ and $8 \times 10^5$ counts per minute. The results are shown in Table 3. Comparable data from the earlier computations have been included in the same table and a slight, but consistent, trend is clearly evident. The computed half-life increases as the counting rate limit is decreased.

A calorimetric determination of the radium-223 half-life with the same material as that used for the alpha-counting determination yielded values of 11.4344 ± 0.0011 and 11.4432 ± 0.0057 days.[14]

The agreement between the calorimetric and alpha-counting results, already quite good for two totally independent methods, appears even better when the lower counting rate limit is imposed. It seems likely that the high precision and probable accuracy of the radium-223 half-life will be useful in elucidating the resolving time behavior of the proportional counter with which the data were obtained.

---

[12]R. T. Birge, *Phys. Rev.*, **40**, 213 (1932).

[13]MLM-1148.

[14]MLM-1135, p. 20.

Table 3

## DECAYING PAIR COMPUTATIONS OF RADIUM-223 HALF-LIFE WITH VARIOUS COUNTING RATE LIMITS[a]

| Counting Rate Limit (cpm) | $T_{1/2}$ ± Ext. P.E. (days) |
|---|---|
| None[b] | 11.4132 ± 0.0051 |
| $3.0 \times 10^6$ | 11.4193 ± 0.0025 |
| $1.3 \times 10^6$ | 11.4228 ± 0.0025 |
| $1.0 \times 10^6$ | 11.4321 ± 0.0019 |
| $0.8 \times 10^6$ | 11.4331 ± 0.0024 |

[a]Data Weighted and Chauvenet's Criterion Used.

[b]Maximum observed counting rate was $3.7 \times 10^6$ cpm.

**Residue Adsorption**

In last month's report, it was noted that a macroscopic impurity was present in the barium-lanthanum-140 received from Oak Ridge, and that the impurity tended to follow the barium-140 through several successive cation exchange purifications. The impurity, which has now been identified spectrographically as "mostly calcium", was finally eliminated by elution with one normal nitric acid from a Dowex-50 cation exchange column.

Continued elution of the column with one normal nitric acid yielded 20 fractions, of which eight, containing most of the barium-140, were evaporated to dryness and examined visually. All fractions had slight visible residues, but they were estimated to be no greater than that to be expected from the reagents.

The barium-140 in the four central fractions was leached from the glass vials with hot demineralized water, passed through a coarse Pyrex frit, and again evaporated to dryness. The nearly invisible residue was taken up in hot demineralized water and made one normal in nitric acid. This solution was now considered satisfactory for residue adsorption experiments.

During the lengthy purification, a number of observations were made which, it is believed, will prove to have been significant. For example, it was found that carrier-free barium-140 could be separated from lanthanum-140 without the use of ammonium hydroxide. If a mixture of the two radioelements is evaporated to dryness from a nitric acid solution and the residue leached with hot distilled or demineralized water, nearly all the barium-140 and a large fraction of the lanthanum-140 are desorbed. However, if the leach solution is passed through a coarse glass frit or a glass wool filter, all of the desorbed lanthanum-140 is adsorbed by the filter, while all but a small fraction of the barium-140 passes through with the solution.

In the work with strontium-yttrium-90 it was found that good separations could be made only from hydroxide residues, because most of the yttrium was desorbed with the strontium from nearly all other types of residue, including nitrates. It is probable that, had the solution been filtered, the yttrium would have been adsorbed by the filter as was the lanthanum in the experiment just described.

A second, and more significant, observation was the reversal of the normal order of adsorption of barium-140 and lanthanum-140. In every case heretofore observed, the rare earth nuclide was more strongly adsorbed than the alkaline earth. However, several instances of reversal were noted following elution of the barium-140 from the Dowex-50 resin and its evaporation to dryness.

The possibility was considered that sufficient radiolytic decomposition of the resin had taken place to release sulfate ion, and that it was the undissociated $BaSO_4$ molecule which was being preferentially adsorbed.

To test this hypothesis, a sample of purified barium-140 from the head end of the last ion exchange elution was evaporated to dryness on a platinum surface, covered with 0.25 milliliter of 0.01 normal sulfuric acid and dried again. The residue was covered with distilled water, dried, and leached successively with hot one normal sulfuric acid, a mixture of 0.8 normal nitric acid and 0.2 normal sulfuric acid, and finally with one normal nitric acid. The distribution of the desorbed radioelements is shown in Table 4, where it is seen that the lanthanum-140 was preferentially desorbed in one normal sulfuric acid and that the barium-140 is readily desorbable in the presence of either a mixture of nitric and sulfuric acids or in nitric acid alone.

The significance of this experiment lies in its confirmation of the basic hypothesis of residue adsorption, *viz.*, that those compounds which are adsorbable are the same as those which, in macroscopic amounts, form precipitates in the corresponding aqueous solutions, and that the same forces that produce precipitates also produce adsorbable "radiocolloids" at the trace level.

**Table 4**

**DESORPTION OF BARIUM-140 AND LANTHANUM-140 SULFATES FROM A PLATINUM SURFACE**

| | Amount Desorbed (%) | |
|---|---|---|
| Leaching Agent | Barium-140 | Lanthanum-140 |
| 1 *N* $H_2SO_4$ | 9.3 | 32.0 |
| 0.8 *N* $HNO_3$ / 0.2 *N* $H_2SO_4$ | 65.7 | 52.1 |
| 1 *N* $HNO_3$ | 24.1 | 15.0 |
| Residual | 0.9 | 1.0 |
| Total (Assumed) | 100 | 100 |

It is interesting to note that, when the experiment was repeated with 0.01 normal sulfuric acid as the first leaching agent, 42 per cent of the barium-140 and 32 per cent of the lanthanum-140 were desorbed, indicating that a fairly high concentration of sulfuric acid is required to maintain the barium sulfate molecule in an undissociated, adsorbable form.

# ISOTOPE SEPARATION

*Processes are being developed for separating and purifying the isotopes of a number of elements including hydrogen, the noble gases, carbon and uranium. Potential sources of supply of these materials are being evaluated.*

## Helium-3

*Vapor Pressure Thermometry* Thermomolecular pressure corrections which will be of use in helium-3 vapor pressure thermometry are being established. The Weber-Schmidt Equation provides the best available predictions for these corrections. This equation is apparently a curve fit on data for unsaturated helium-4 vapor. It has been found valid for unsaturated helium-3 vapor in the limited experiments of Roberts and Sydoriak.

Published helium-3 and helium-4 vapor pressure data are being computed by the Weber-Schmidt Equation.[15] to obtain the predicted thermomolecular pressure corrections on saturated vapor as a function of temperature for a number of pressure sensing tube diameters. When these data are plotted (Figure 1) the positions of the relative maximum, and especially the relative minimum, move upwards and to the right as the tube diameter decreases. The curves tend to converge at the high and low temperature ends. Two notable features of these curves are that the greatest absolute correction is not predicted to be at the lowest temperature and that the absolute correction tends to approach zero with the temperature increasing to the normal boiling point.

*Analysis of Tritium in Helium-3* In recent analyses of tritium in helium-3, Geiger tubes prepared at Mound Laboratory yielded plateaus as shown in Figure 2. If the plateau followed a peak, as shown in the drawing the region at (C) was used for analysis. (The dotted line indicates a normal plateau.) In some cases the plateau in that region was only 25 volts wide. To determine the reason for the peak shown at (B) the isobutane content of the counting gas in the Geiger was varied from two to 12 per cent in one per cent increments. At seven per cent isobutane, the plateaus were shaped normally but were only 50 to 100 volts in length and usually started at 2300 volts. This high level became a problem since the presently used scaler has a maximum output of 2500 volts. With samples of high count rates, the plateaus would be at a high voltage greater than could be supplied by the scaler. Therefore, varying the gas content was not a satisfactory solution.

The pulses from the counting tubes filled with 98 per cent helium two per cent isobutane were measured with an oscilloscope; these pulses were 10 to 15 volts in height with a 45-microsecond decay time. As the voltage increased, a secondary pulse of about four volts developed in Geiger-Muller input circuit. Thus, the shape of the plateau in Figure 2 was explained by the secondary pulse. As the voltage increased to region (A) in Figure 2, an increasing number of primary pulses were counted (Figure 3A). From region (A) to (B) in Figure 2, all primary pulses were counted, and an increasing number of secondary pulses were large enough to be counted (Figure 3B). From region (B) to (C) the primary pulses increased in height and decay time to the point at which the secondary pulses were not counted (Figure 3C). Beyond region (C) gas breakdown occurred.

The problem was corrected by modifying the G.M. input circuit. A $10^5$-ohm resistor was added in series with the existing 68,000-ohm resistor to attenuate the pulses, and a 56-$\mu\mu$f capacitor was added in parallel with the existing 47-$\mu\mu$f capacitor to eliminate the secondary pulse. As a result the plateaus start at 1300 volts, are 100 to 200 volts long, and have a zero slope (Figure 4) at the best 50-volt interval.

[15]Roberts and Sydoriak, *Phys. Rev.*, **102**, 305 (1956).

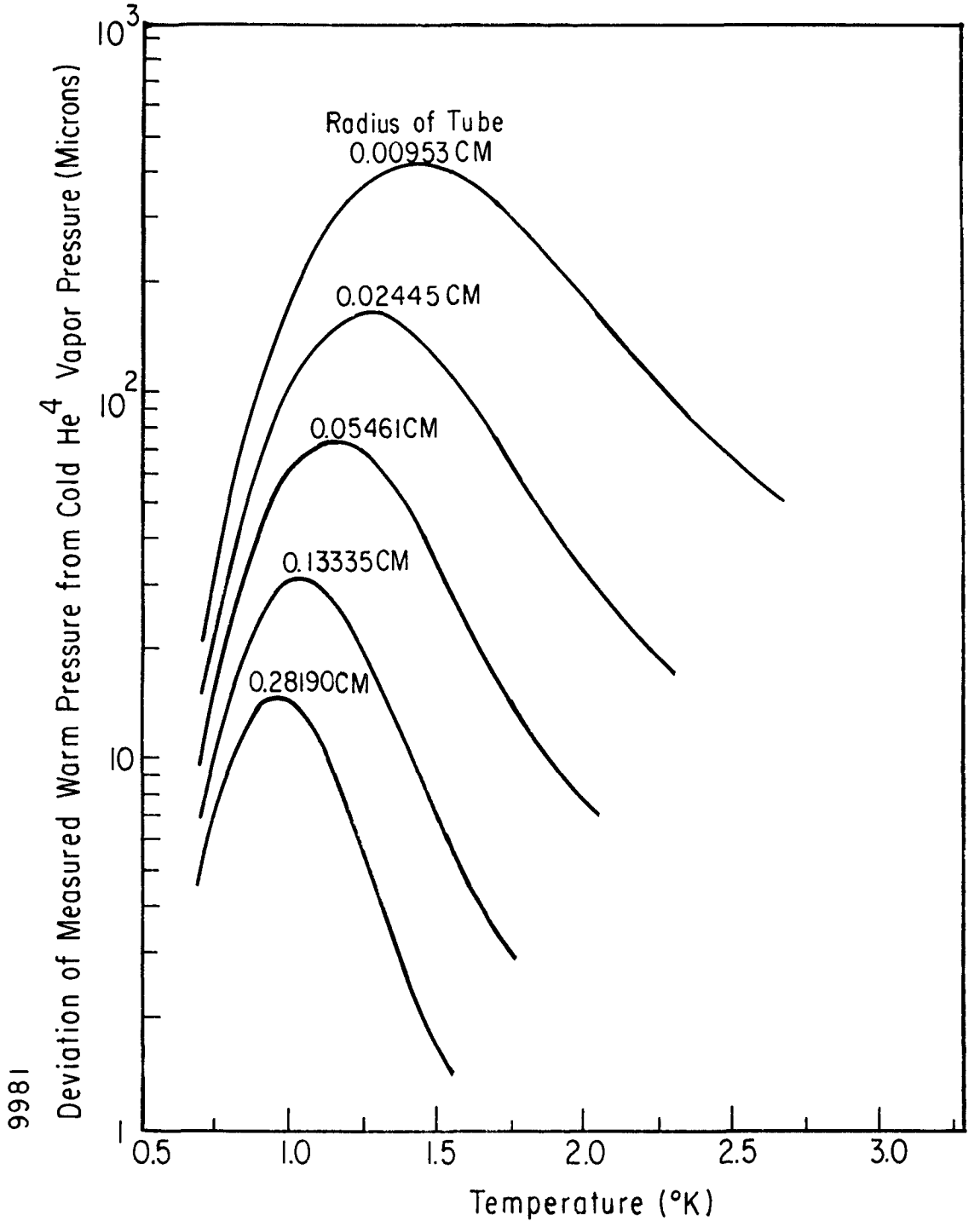


**Figure 1.** *Helium-4 Thermomolecular Pressure Corrections According to the Weber-Schmidt Equation.*

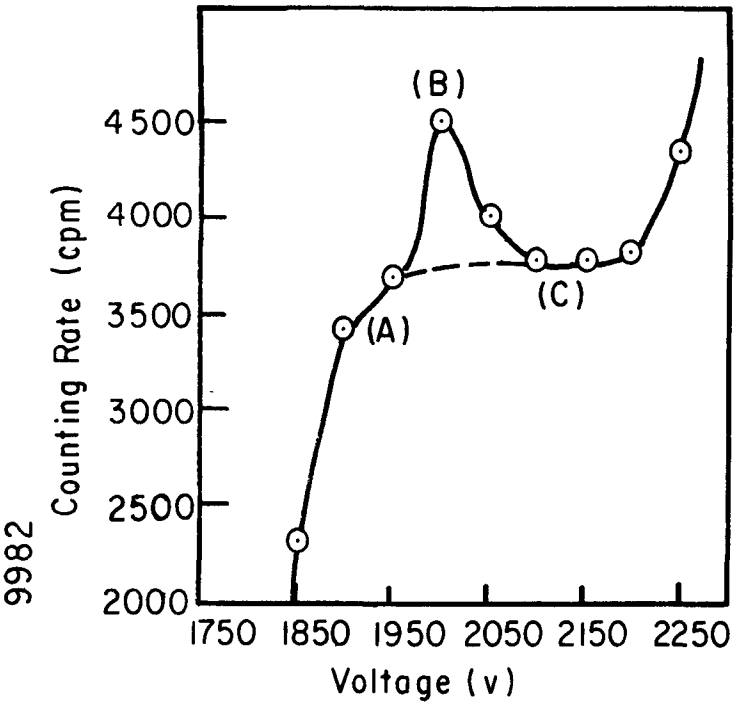


**Figure 2.** *Geiger-Muller Counting Rate as a Function of High Voltage.*

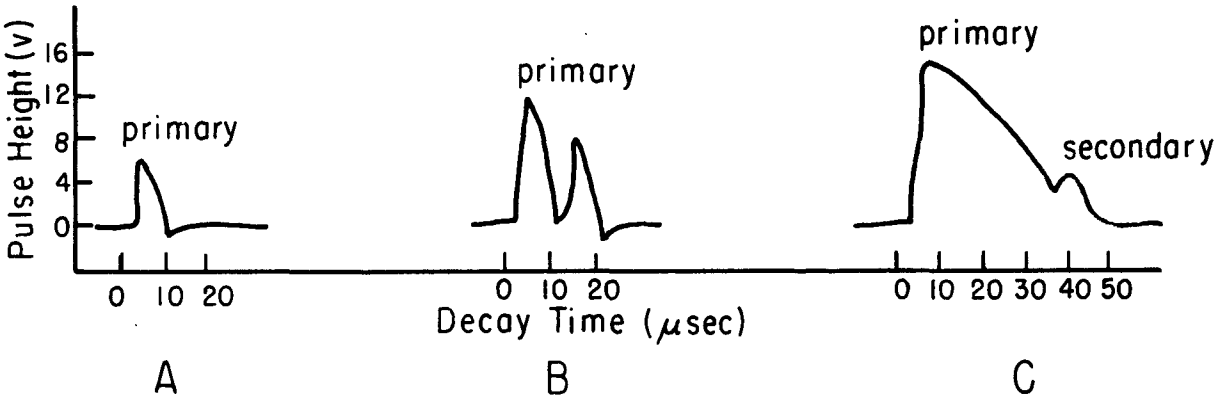


**Figure 3.** *Geiger-Muller Pulse Size and Shape.*

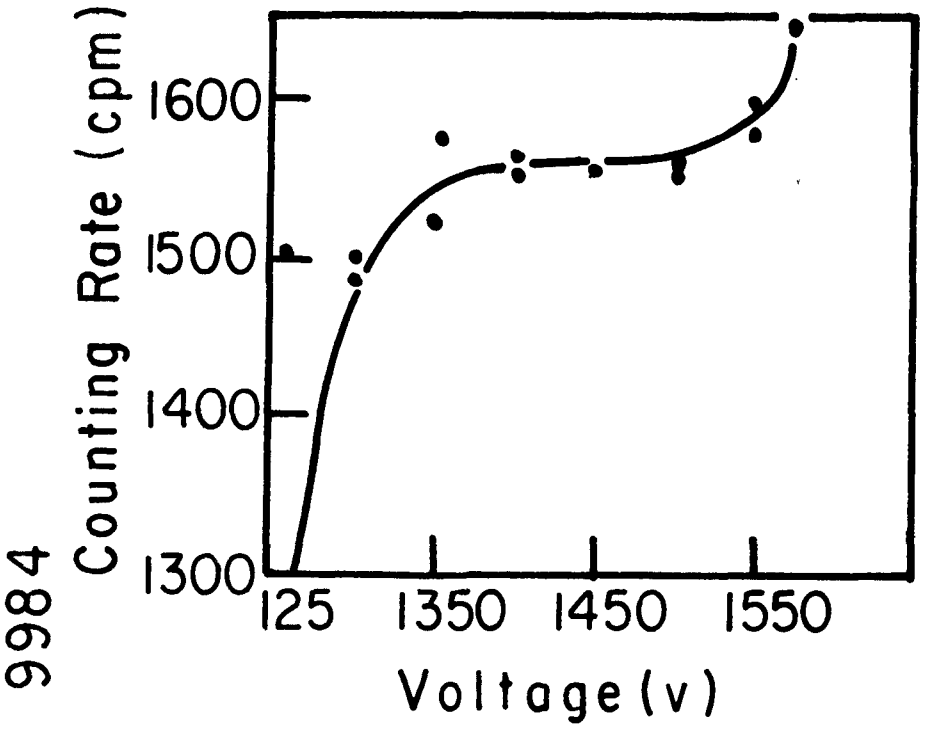


**Figure 4.** *Normal Pulse From Modified Circuit.*

**Equation of Continuity for the Cylindrical Case**

The Equation of Continuity for Species 1 may be derived from a mass balance over a differential volume element fixed with respect to the coordinates of the column.

$$\text{Net rate of change of mass in volume element} = \text{Mass flux in - Mass flux out}$$

In terms of the density of the fluid, this may be written as:

$$\frac{\partial}{\partial t} m_1 n_1 = -(\nabla \cdot n_1 m_1 \vec{v})$$

where the vector $m_1 n_1 \vec{v}$ is the mass flux relative to the fixed coordinate system. The mass flux vector relative to the stream velocity for Species 1, usually called $\vec{j}_1$ when expressed as gradients of the concentration and pressure, and the external forces, is

$$\vec{j} = n_1 m_1 \vec{V} = \frac{n^2}{\rho} m_1 m_2 D_{12} \vec{d}_2 - D_1^T \nabla \ln T$$

This is the molecular flux due to ordinary and thermal diffusion, and it is relative to the stream velocity which is assumed to flow in the vertical direction only.

It may be noted that $\vec{j}_1 = -\vec{j}_2$, $\vec{d}_1 = -\vec{d}_2$, $D_{12} = D_{21}$, $D_1^T = -D_2^T$; then the equation is expressed in terms of Component 1:

$$\vec{d}_1 = \nabla c_1 + (c_1 - \frac{n_1 m_1}{\rho})\nabla p - (\frac{n_1 m_1}{p\rho})\left[\frac{\rho}{m}\vec{X} - n_1\vec{X} - n_2\vec{X}\right]$$

In $\vec{d}_1$ it is seen that the term due to the pressure gradient is negligible since separation due to gravity alone is small. This effect can be magnified by use of an ultra-centrifuge. The only external force on the system is gravity. Since this is an acceleration the term vanishes by virtue of Newton's First Law, $\vec{F}_i = m_i \vec{a}$, and

$$\frac{n_1 m_1}{p\rho}\left[\frac{\rho}{m_1}\vec{X} - n_1\vec{X} - n_2\vec{X}\right] = \frac{n_1 m_1}{p\rho}\left[(n_1 m_1 + n_2 m_2)\vec{g} - (n_1 m_1 + n_2 m_2)\vec{g}\right] = 0$$

If the "thermal diffusion ratio" is defined as

$$k_T = \frac{\rho}{n^2 m_1 m_2}\frac{D_1^T}{D_{12}}$$

the total flux for component 1 relative to the fixed coordinate system may then be written as follows:

$$\vec{J}_1 = n_1 m_1 (\vec{v} + \vec{V}_1) = n_1 m_1 \vec{v} - \frac{n^2}{\rho} m_1 m_2 D_{12}\nabla c_1 - D_1^T \nabla \ln T$$

This expression may be factored by using the expression for $k_T$ and the fact that $c_1 = n_1/n$ thus,

$$\vec{J}_1 = n m_1 \left[c_1 \vec{v} - \frac{n m_2}{\rho} D_{12}(\nabla c_1 + k_T \nabla \ln T)\right]$$

In the Equation of Continuity the time derivative is taken to be zero for the steady state, leaving

$$\text{div } \vec{J}_1 = \text{div } \vec{J}_2 = 0$$

for the two components. The mass $m_1$ is constant and may be factored out immediately. Since the stream velocity is in the $z$ direction only, the divergence of this term yields

$$\nabla \cdot n c_1 \vec{v} = \frac{\partial}{\partial z}(n c_1 v_z)$$

The divergence of the concentration gradient has a contribution in both the radial direction and the $z$ direction due to ordinary diffusion. The concentration gradient in the $r$ direction, which is due to thermal diffusion, is very small, but it is necessary and must be retained in the analysis. The $z$ component of the divergence is due to longitudinal back diffusion and limits the overall enrichment in the column.

$$\nabla \cdot (-\frac{n^2 m_2 D_{12}}{\rho}\nabla c_1) = -m_2\left[\frac{1}{r}\frac{\partial}{\partial r}\left(\frac{r n^2 D_{12}}{\rho}\frac{\partial c_1}{\partial r}\right) + \frac{\partial}{\partial z}\left(\frac{n^2 D_{12}}{\rho}\frac{\partial c_1}{\partial z}\right)\right]$$

Thermal diffusion acts essentially only in the radial direction, thus the final term is

$$\nabla \cdot (-\frac{n^2 m_2 D_{12} k_T}{\rho}\nabla \ln T) = -m_2\left[\frac{1}{r}\frac{\partial}{\partial r}\left(\frac{r n^2 D_{12} k_T}{\rho}\frac{\partial \ln T}{\partial r}\right)\right]$$

These terms are collected and grouped with $z$-dependent terms on one side and $r$-dependent terms on the other. This may be interpreted as a balance of the divergences of the flux in the $r$ and $z$ directions which is mandatory if the overall system has no sources or sinks.

$$\nabla \cdot \vec{J} = 0$$

$$\frac{\partial}{\partial z} J_{1z} = -\frac{1}{r} \frac{\partial}{\partial r} r J_{1r}$$

or

$$\frac{m_2}{r} \frac{\partial}{\partial r} \frac{r n^2 D_{12}}{\rho} \left[ \frac{\partial c_1}{\partial r} + k_T \frac{\partial \ln T}{\partial r} \right] = \frac{\partial}{\partial z} (n c_1 v_z) - m_2 \frac{\partial}{\partial z} \left( \frac{n^2 D_{12}}{\rho} \frac{\partial c_1}{\partial z} \right)$$

If both sides of the general equation are multiplied by $rdr$ and integrated from the wire to any point $r$ in the column, the following is obtained:

$$\frac{r n^2 m_2 D_{12}}{\rho} \left[ \frac{\partial c_1}{\partial r} + k_T \frac{\partial \ln T}{\partial r} \right] \Bigg|_{r_2}^{r} = \int_{r_2}^{r} \frac{\partial}{\partial z} (n c_1 v_z) r dr$$

$$- m_2 \int_{r_2}^{r} \frac{\partial}{\partial z} \left( \frac{n^2 D_{12}}{\rho} \frac{\partial c_1}{\partial z} \right) r dr$$

The radial part of the flux is

$$J_{1r} = -\frac{n^2 m_1 m_2 D_{12}}{\rho} \left[ \frac{\partial c_1}{\partial r} + k_T \frac{\partial \ln T}{\partial r} \right]$$

This flux must be identically zero at the wire and the wall. Since the radial part of the differential equation differs from the flux only by a proportionality factor $-r/m_1$, the lower limit of the left-hand side of the integrated equation above is zero. Thus, a concentration profile may be obtained as a function primarily of the radial temperature distribution with smaller contributing terms which are functions of the longitudinal concentration gradient.

$$\frac{\partial c_1}{\partial r} = -k_T \frac{\partial \ln T}{\partial r} + \frac{\rho}{r n^2 m_2 D_{12}} \int_{r_2}^{r} \frac{\partial}{\partial z} (n c_1 v_z) r dr$$

$$- \frac{\rho}{r n^2 D_{12}} \int_{r_2}^{r} \frac{\partial}{\partial z} \left( \frac{n^2 D_{12}}{\rho} \frac{\partial c_1}{\partial z} \right) r dr$$

An integration with respect to $r$ yields

$$c_1(r, z) = -\int_{r_1}^{r} \frac{k_T}{T} \frac{\partial T}{\partial r} dr + \frac{1}{m_2} \int_{r_2}^{r} \frac{\rho}{r n^2 D_{12}} \int_{r_2}^{r} r \frac{\partial}{\partial z} (n c_1 v_z) dr^2$$

$$- \int_{r_2}^{r} \frac{\rho}{r n^2 D_{12}} \int_{r_2}^{r} r \frac{\partial}{\partial z} \left( \frac{n^2 D_{12}}{\rho} \frac{\partial c_1}{\partial z} \right) dr^2 + K_1$$

This equation may be averaged at a given level of $z$ by integrating over $r_2 \rightarrow r_1$. Although the transport properties are expressed as functions of temperature, it is noteworthy that the averaging process cannot be accomplished exactly by integration over $T$ due to a slight skewing of the $T$ versus $Z$ coordinate system, which arises from a varying wire temperature. This skewing does not disrupt the calculation of the profile as a function of temperature, but requires only that the averaging process be performed in an orthogonal system.

The averaging of the concentration profile in cylindrical coordinates must be done by integrating over the area in the column at a given level.

$$\bar{c}_1(z) = \frac{\int_0^{2\pi} \int_{r_2}^{r_1} c_1(r,z)\, r \, dr d\theta}{\int_0^{2\pi} \int_{r_2}^{r_1} r \, dr \, d\theta} = \frac{2}{r_1^2 - r_2^2} \int_{r_2}^{r_1} c_1(r,z)\, r dr$$

Insertion of the expression for $c_1(r,z)$ yields

$$\bar{c}_1(z) = - \frac{2}{r_1^2 - r_2^2} \int_{r_2}^{r_1} r \int_{r_2}^{r} \frac{kT}{T} \frac{\partial T}{\partial r} dr^2$$

$$+ \frac{2}{m_2 (r_1^2 - r_2^2)} \int_{r_2}^{r_1} r \int_{r_2}^{r} \frac{\rho}{r n^2 D_{12}} \int_{r_2}^{r} r \frac{\partial}{\partial z} (n c_1 v_z) dr^3$$

$$- \frac{2}{r_1^2 - r_2^2} \int_{r_2}^{r_1} r \int_{r_2}^{r} \frac{\rho}{r n^2 D_{12}} \int_{r_2}^{r} r \frac{\partial}{\partial z} \left( \frac{n^2 D_{12}}{\rho} \frac{\partial c_1}{\partial z} \right) dr^3 + K1$$

The constant $K1$ may be evaluated by means of this last equation from which the final expression for the concentration profile is obtained:

$$K1 = \bar{c}_1(Z) + \delta(Z)$$

Therefore,

$$c_1(r, z) = \bar{c}_1(z) + \delta(z) - a_1(r, z) + a_2(r, z) - a_3(r, z)$$

It should be remembered that the final expression for $c_1(r, z)$ is not explicit since the variable is present implicitly in each of the terms on the right-hand side of the equation. Thus, the equation is not suitable for computational purposes without appropriate manipulation and approximations.

The terms containing $k_T$ have a primary concentration dependence of the form $c_1(1-c_1)$ since the first approximation to the thermal diffusion ratio is

$$[k_T]_1 = \frac{c_1 c_2}{6[\lambda_{12}]_1}\left\{\frac{S^{(1)}c_1 - S^{(2)}c_2}{X_\lambda + Y_2}\right\}(6C_{12}^* - 5) = c_1(1-c_1)\alpha$$

where the functions $S^{(1)}$, $S^{(2)}$, $X_\lambda$, $Y_\lambda$, and $C_{12}^*$ are defined by Hirschfelder, Curtiss, and Bird;[16] for their nomenclature (as opposed to Jones and Furry) the value of $K_T$ will be negative in cases where Species 1 concentrates at the hot wire. The primary concentration dependence of $k_T$ may be factored out, leaving the "thermal diffusion factor" which is only weakly concentration dependent.

$$\alpha = \frac{1}{6[\lambda_{12}]_1}\left\{\frac{S^{(1)}c_1 - S^{(2)}c_2}{X_\lambda - Y_\lambda}\right\}(6C_{12} - 5)$$

The quantities $\delta$, $a_1$, $a_2$, and $a_3$ may now be defined:

$$\delta(z) = \frac{2}{(r_1^2 - r_2^2)}\int_{r_2}^{r_1} r \int_{r_2}^{r} \frac{c_1(1-c_1)\alpha}{T}\frac{\partial T}{\partial r}\,dr^2$$

$$- \frac{2}{m_2(r_1^2 - r_2^2)}\int_{r_2}^{r_1} r \int_{r_2}^{r} \frac{\rho}{rn^2 D_{12}}\int_{r_2}^{r} r\frac{\partial}{\partial z}(nc_1 v_z)\,dr^3$$

$$+ \frac{2}{(r_1^2 - r_2^2)}\int_{r_2}^{r_1} r \int_{r_2}^{r} \frac{\rho}{rn^2 D_{12}}\int_{r_2}^{r} r\frac{\partial}{\partial z}\left(\frac{n^2 D_{12}}{\rho}\frac{\partial c_1}{\partial z}\right)dr^3$$

$$a_1(r_1 z) = \int_{r_2}^{r} \frac{c_1(1-c_1)\alpha}{T}\frac{\partial T}{\partial r}\,dr$$

$$a_2(r, z) = \frac{1}{m_2}\int_{r_2}^{r} \frac{\rho}{rn^2 D_{12}}\int_{r_2}^{r} r\frac{\partial}{\partial z}(nc_1 v_z)\,dr^2$$

$$a_3(r, z) = \int_{r_2}^{r} \frac{\rho}{rn^2 D_{12}}\int_{r_2}^{r} r\frac{\partial}{\partial z}\left(\frac{n^2 D_{12}}{\rho}\frac{\partial c_1}{\partial z}\right)dr^2$$

Since the radial concentration profile has been determined as established essentially by thermal diffusion and modified by small side effects, the original flux equation is now used to obtain the longitudinal equation:

$$\frac{\partial}{\partial z}J_{1z} = -\frac{1}{r}\frac{\partial}{\partial r}rJ_{1r}$$

[16] J. O. Hirschfelder, C. F. Curtiss, and R. B. Bird, *Molecular Theory of Gases and Liquids*, New York, John Wylie, 1954, p. 541.

If this equation is multiplied through by $r$ and integrated from $r_2 \to r_1$, the right-hand side is zero from the boundary conditions at the wire and the wall.

$$\int_{r_2}^{r_1} \frac{\partial}{\partial z}\, r J_{1z}\, dr = \Big[ r J_{1r} \Big]_{r_2}^{r_1} \equiv 0$$

This equation may now be integrated once with respect to $z$:

$$\int_{r_2}^{r_1} J_{1z}\, r dr = K2$$

Here it may be recognized that the flux in the $z$ direction integrated over the cross section of the column is just the net transport of species 1. This is usually referred to as $r_1$ and is zero for the present case of no draw-off.

$$r_1 = 2\pi\, m_1 \int_{r_2}^{r_1} n c_1 v_z\, r dr - 2\pi m_1 m_2 \int_{r_2}^{r_1} \frac{n^2 D_{12}}{\rho} \frac{\partial c_1}{\partial z}\, r dr$$

The complete expression for the transport is obtained by substituting the previously derived expression for $c_1(r,z)$ in the above equation:

$$r_1 = 2\pi\, m_1 \int_{r_2}^{r_1} n v_z\, [\bar{c}_1 + \delta(z)]\, r dr - 2\pi m_1 \int_{r_2}^{r_1} n v_z\, a_1(r,z)\, r dr$$

$$+ 2\pi\, m_1 \int_{r_2}^{r_1} n v_z\, [a_2(r,z) - a_3(r,z)]\, r dr$$

$$- 2\pi\, m_1 m_2 \int_{r_2}^{r_1} \frac{n^2 D_{12}}{\rho} \left[ \frac{\partial \bar{c}_1}{\partial z} + \frac{\partial \delta(z)}{\partial z} \right] r dr$$

$$+ 2\pi\, m_1 m_2 \int_{r_2}^{r_1} \frac{n^2 D_{12}}{\rho} \frac{\partial}{\partial z} [a_1(r,z) - a_2(r,z) + a_3(r,z)]\, r dr$$

This equation and the equation for $c_1(r,z)$, form a coupled set of equations whose solution yields the concentration distribution in the column. Although the equations are exact, they are not yet in a form which can be readily handled. It will be helpful to rearrange the equation so that terms which contribute a major effect stand alone, while smaller correction terms are combined in certain groupings in order to provide a comparison with previous theories. The second and third terms in the equation above may be integrated by parts:

$$\int_{r_2}^{r_1} u\, dv = uv \Big|_{r_2}^{r_1} - \int_{r_2}^{r_1} v\, du$$

where

$$u = a_1(r,z) \qquad v = \int_{r_2}^{r} m_1 n v_z r dr$$

$$du = d a_1 = c_1 c_2 \frac{a}{T} \frac{\partial T}{\partial r} dr \qquad dv = m_1 n v_z r dr$$

Therefore,

$$\int_{r_2}^{r_1} a_1(r,z) m_1 n v_z r dr = \left| a_1(r,z) \int_{r_2}^{r} m_1 n v_z r dr \right|_{r_2}^{r_1} - \int_{r_2}^{r_1} c_1 c_2 \frac{a}{T} \frac{\partial T}{\partial r} \int_{r_2}^{r} m_1 n v_z r dr^2$$

$$= a_1(r_1,z)\, G(r_1) - \int_{r_2}^{r_1} c_1 c_2 \frac{a}{T} \frac{\partial T}{\partial r} G(r)\, dr$$

when $G(r)$ is the frequently occurring integral:

$$G(r) = \int_{r_2}^{r} m_1 n v_z r dr$$

The third term integrates as follows:

$$u = a_2(r,z) - a_3(r,z) \qquad v = \int_{r_2}^{r} m_1 n v_z r dr$$

$$du = da_2 - da_3 \qquad dv = m_1 n v_z r dr$$

$$du = \frac{\rho}{m_2 r n^2 D_{12}} \int_{r_2}^{r} r \frac{\partial}{\partial z} (n c_1 v_z)\, dr$$

$$- \frac{\rho}{r n^2 D_{12}} \int_{r_2}^{r} r \frac{\partial}{\partial z} \left( \frac{n^2 D_{12}}{\rho} \frac{\partial c_1}{\partial z} \right) dr$$

Therefore,

$$\int_{r_2}^{r_1} m_1 n v_z (a_2 - a_3) r dr = \left| [a_2(r,z) - a_3(r,z)] \int_{r_2}^{r} m_1 n v_z r dr \right|_{r_2}^{r_1}$$

$$- \int_{r_2}^{r_1} \left[ \int_{r_2}^{r} m_1 n v_z \, r dr \right] \frac{\rho}{m_2 r n^2 D_{12}} \int_{r_2}^{r} r \frac{\partial}{\partial z} (n c_1 v_z) \, dr^2$$

$$+ \int_{r_2}^{r_1} \left[ \int_{r_2}^{r} m_1 n v_z \, r dr \right] \frac{\rho}{r n^2 D_{12}} \int_{r_2}^{r} r \frac{\partial}{\partial z} \left( \frac{n^2 D_{12}}{\rho} \frac{\partial c_1}{\partial z} \right) dr^2$$

$$= [a_2(r_1, z) - a_3(r_1, z)] \, G(r_1)$$

$$- \int_{r_2}^{r_1} \frac{G(r) \rho}{m_2 r n^2 D_{12}} \frac{\partial}{\partial z} \int_{r_2}^{r} r n c_1 v_z \, dr^2$$

$$+ \int_{r_2}^{r_1} \frac{G(r) \rho}{r n^2 D_{12}} \frac{\partial}{\partial z} \int_{r_2}^{r} \frac{r n^2 D_{12}}{\rho} \frac{\partial c_1}{\partial z} \, dr^2$$

Substitution of the results of the partial integrations into the transport equation and rearrangement yields:

$$r_1 = 2\pi \int_{r_2}^{r_1} c_1 (1 - c_1) \frac{a}{T} \frac{\partial T}{\partial r} G(r) dr - 2\pi \int_{r_2}^{r_1} \frac{\rho}{m_1 m_2 r n^2 D_{12}} G(r) \frac{\partial}{\partial z} c_1 G(r) \, dr$$

$$-2\pi m_1 m_2 \frac{\partial \bar{c}_1}{\partial z} \int_{r_2}^{r_1} \frac{n^2 D_{12}}{\rho} r dr + 2\pi \int_{r_2}^{r_1} \frac{G(r) \rho}{r n^2 D_{12}} \frac{\partial}{\partial z} \int_{r_2}^{r} \frac{r n^2 D_{12}}{\rho} \frac{\partial c_1}{\partial z} \, dr^2$$

$$+ 2\pi m_1 \int_{r_2}^{r_1} n v_z [\bar{c}_1 + \delta(z)] r dr + 2\pi G(r_1) [-a_1(r_1) + a_2(r_1) - a_3(r_1)]$$

$$- 2\pi m_1 m_2 \int_{r_2}^{r_1} \frac{n^2 D_{12}}{\rho} \frac{\partial}{\partial z} [\delta(z) - a_1(r, z) + a_2(r, z) - a_3(r, z)] r dr$$

The expression for the transport of species 1 up the column has been rigorous up to this point. However, it is difficult to handle this equation in its present form since it contains the concentration as a function of both $r$ and $z$. One method of overcoming this problem is to neglect the variation of the concentration in the radial direction, i.e., replace $c_1(r, z)$ by $\bar{c}_1(z)$. Since the separation in the radial direction is very small,

$$\Delta c_1 = c_1(r_2, z) - c_1(r_1, z) \sim \bar{c}_1 \bar{c}_2 \alpha \ln \left( T_2 / T_1 \right),$$

the fractional error introduced by neglecting the radial variation of the concentration is very small. Using this approximation, the preceding equation reduces to the following:

$$r_1 = 2\pi \bar{c}_1 \bar{c}_2 \int_{r_2}^{r_1} \frac{a}{T} \frac{\partial T}{\partial r} G(r) dr - \frac{d \bar{c}_1}{dz} \int_{r_2}^{r_1} \frac{\rho}{m_1 m_2 r n^2 D_{12}} [G(r)]^2 \, dr$$

$$-2\pi\ \bar{c}_1 \int_{r_2}^{r_1} \frac{\rho G(r)}{m_1 m_2\, r n^2 D_{12}} \cdot \frac{\partial}{\partial z}\, G(r)\, dr \;-2\pi\ \frac{d\bar{c}_1}{dz} \int_{r_2}^{r_1} \frac{m_1 m_2 n^2 D_{12}}{\rho}\, r dr$$

$$+2\pi\ \frac{d^2\bar{c}}{dz^2} \int_{r_2}^{r_1} \frac{G(r)\,\rho}{r n^2 D_{12}} \int_{r_2}^{r} \frac{r n^2 D_{12}}{\rho}\, dr^2$$

$$+\ 2\pi\ \frac{d\bar{c}_1}{dz} \int_{r_2}^{r_1} \frac{G(r)}{r n^2 D_{12}}\, \rho \int_{r_2}^{r} \frac{\partial}{\partial z}\ \frac{n^2 D_{12}}{\rho}\, r dr^2$$

$$+\ 2\pi\ \bar{c}_1 \int_{r_2}^{r_1} n v r\, dr$$

In obtaining this equation, the following relation was used:

$$c_1(r,z) = \bar{c}_1 + \delta - a_1 + a_1 - a_3 \sim \bar{c}_1$$

It is of interest to note that if the transport properties are assumed to be independent of concentration, this equation reduces to

$$r_1 = 2\pi\ \bar{c}_1 \bar{c}_2 \int_{r_2}^{r_1} \frac{a}{T}\ \frac{\partial T}{\partial r}\, G(r)\, dr \;-2\pi\ \frac{d\bar{c}_1}{dz} \int_{r_2}^{r_1} \frac{[G(r)]^2}{r\rho D}\ dr$$

$$-\ 2\pi\ \frac{d\bar{c}_1}{dz} \int_{r_2}^{r_1} \rho D\, r dr + 2\pi\ \frac{d^2\bar{c}}{dz^2} \int_{r_2}^{r_1} \frac{G(r)}{r\rho D} \int_{r_2}^{r} r\rho D\ dr^2$$

where each of the integrals are constants independent of $r$ and $z$. Except for the last term, this is the transport equation obtained by Jones and Furry. Saxena has shown that the fractional error introduced by neglecting this term is approximately one per cent.[17]

For a mixture of light isotopes, the assumption that the transport properties are independent of concentration is not valid. For this case, the transport equation contains three additional terms. Also, the integrals are functions of both the concentration and the $z$ coordinate (They are functions of $z$ because both the concentration and temperature are functions of $z$). The concentration dependence can be removed from some of the integrals by expanding the quantity

$$\frac{n}{\rho} = \frac{1}{m_1 c_1 + m_2 c_2}$$

in a Taylor series about $m_2 = m_1$, obtaining,

$$\frac{n}{\rho} = \frac{1}{m_2} + \frac{(m_2 - m_1)}{m_2^2}\ c_1 + \frac{(m_2 - m_1)^2}{m_2^3}\ c_1^2 +$$

[17] S. C. Saxena, *Revs. Mod. Phys.*, **34**, 252-66 (1962).

and

$$\int_{r_2}^{r_1} \frac{m_1 m_2 n^2 D}{\rho}\, r dr \simeq \left[1 + \frac{(m_2 - m_1)}{m_2}\,\bar{c}_1\right] \int_{r_2}^{r_1} m_1 n D r dr$$

The integral on the right-hand side is independent of the concentration.

Also, consider the integral

$$K_i(z) = \int_{r_2}^{r_1} \frac{G(r)\rho}{r n^2 D} \int_{r_2}^{r} \frac{\partial}{\partial z}\,\frac{n^2 D}{\rho}\, r dr^2$$

Since this integral appears in a term which is small (compared to the terms containing $d\bar{c}_1/dz$), any small error introduced in evaluating this integral will appear as a much smaller error in the final results. Specifically, neglecting the $z$ dependence of the temperature in the quantity $(nD)$, the integral is

$$K_i(z) = \int_{r_2}^{r_1} \frac{G(r)\rho}{r n^2 D} \int_{r_2}^{r} nD\,\frac{\partial}{\partial z}\,\frac{n}{\rho}\, r dr^2$$

$$= \frac{d\bar{c}_1}{dz}\,\frac{(m_2 - m_1)}{m_2^2} \int_{r_2}^{r_1} \frac{G(r)\rho}{r n^2 D} \int_{r_2}^{r} n D r dr^2$$

Substituting these last two results into the transport equation,

$$r_1 = \bar{c}_1 [H(z) + H'(z)] - \bar{c}_1^2 H(z)$$
$$- \frac{d\bar{c}_1}{dz}\left[K_c(z) + K_d(z)\left\{1 + \frac{(m_2 - m_1)}{m_2}\,\bar{c}_1\right\} - \frac{d\bar{c}_1}{dz}\,\frac{(m_2 - m_1)}{m_2^2}\,K_i(z)\right]$$
$$+ \frac{d^2\bar{c}_1}{dz^2}\,K_l(z)$$

where

$$H(z) = 2\pi \int_{r_2}^{r_1} \frac{a}{T}\,\frac{\partial T}{\partial r}\, G(r)\, dr$$

$$H'(z) = 2\pi \int_{r_2}^{r_1} n m_1 v r dr - 2\pi \int_{r_2}^{r_1} \frac{G(r)\rho}{r n^2 m_1 m_2 D}\,\frac{\partial}{\partial z}\, G(r)\, dr$$

$$K_c(z) = 2\pi \int_{r_2}^{r_1} \frac{[G(r)]^2 \rho}{r n^2 m_1 m_2 D}\, dr$$

$$K_i(z) = 2\pi \int_{r_2}^{r_1} \frac{G(r)\,\rho}{r n^2 D} \int_{r_2}^{r} n D r\, dr^2$$

$$K_c(z) = 2\pi \int_{r_2}^{r_1} \frac{G(r)\,\rho}{r n^2 D} \int_{r_2}^{r} \frac{r n^2 D}{\rho}\, dr^2$$

$$K_d(z) = 2\pi \int_{r_2}^{r_1} m_1 n D r\, dr$$

All of these integrals, except the last one, are functions of the concentration. In order to remove this dependence, the functional dependence of $G(r)$ on the concentration must be known. The problem of determining the functional dependence of $G(r)$ on $\bar{c}_1$ is currently being studied.

## Carbon-13

The objectives of the carbon-13 program are the preparation of gram quantities of 90 per cent purity carbon-13, the evaluation of carbon monoxide and methane as feed materials to the thermal diffusion separation systems, and the evaluation of various other separation methods, such as chemical exchange and distillation.

*Thermal Diffusion* The thermal diffusion cascade for the separation of carbon-13 from natural abundance methane was increased from 10 to 11 columns. After six days the reported mass-17 enrichment at the middle of the last column had reached 97.9 per cent in methane of 53.7 per cent purity. At the top of the last column the enrichment was 96.5 per cent in methane of 95.7 per cent purity. Two days later product withdrawal was started at the rate of 25 milliliters per day from the top of the last column.

*Measurement of Carbon Monoxide Transport Coefficients* Complete experimental thermal diffusion column transport data have been obtained for carbon monoxide with a wire temperature of 500°C. Complete static data and partial flow data have been obtained for a wire temperature of 350°C. Column transport coefficients were computed from the 500°C data. The coefficients which best fit the experimental data are given in Table 5. Theoretical values of the coefficients derived from the shape factor tabulation of McInteer and Reisfeld[16] are also given in Table 5. The coefficients are defined by the following differential equation for isotope transport in a gaseous thermal diffusion column:

$$r = H' p^2 c\,(1-c) - (K_c' p^4 + K_d)\,\frac{dc}{dz}$$

where $r$ is the rate of transport of the desired isotope toward the positive end of the column, $p$ is the pressure, $c$ is the fraction of the desired isotope, and $z$ is the vertical coordinate. The agreement between theoretical and experimental values of the column transport coefficients is satisfactory, even though carbon monoxide does not conform strictly to the assumptions of the theoretical treatment.

*Distillation of Carbon Monoxide* The length of a distillation column is a function of three factors: 1) actual theoretical stage requirement, 2) height equivalent to one theoretical stage, and 3) average relative volatility. With these three factors related to boilup rate a method was developed to select the optimum throughput for any given carbon-13 production rate, i.e., the throughput rate which results in a minimum length column for

[16] B. B. McInteer and M. J. Reisfeld, LAMS-2517 (Feb. 1961).

the given separation. The first factor, actual theoretical stage requirement, can be related to throughput through the correlation of Gilliland or of Erbar and Maddox, which relate actual to minimum theoretical stage requirements as a function of the relation between actual and minimum reflux ratios. The second factor, height equivalent to one theoretical stage, is a direct function of boilup and a measurable characteristic of the type of column selected. The third factor, average relative volatility, a property of the components to be separated and an inverse function of pressure, can be related to average column pressure which is a function of head pressure and column pressure drop; the last is, in turn, a function of the column selected and the boilup rate. Minimum theoretical stage requirements (Figure 5) were used as a basis for optimizing the first two factors. When minimum theoretical stages are known:

$$\text{Column length} = Sm \times S/S_m \times HETP$$

where $Sm$ = minimum theoretical stages

$S/S_m$ = ratio of actual theoretical stages/minimum theoretical stages

$HETP$ = height equivalent to one theoretical plate (or stage)

**Table 5**

**THEORETICAL AND EXPERIMENTAL VALUES OF THERMAL DIFFUSION COLUMN TRANSPORT COEFFICIENTS FOR MASS 29 CARBON MONOXIDE AT A WIRE TEMPERATURE OF 500°C**

Cold Wall Diameter - 3/4 inch

Cold Wall Temperature - 15°C

Hot Wall Diameter - 1/16 inch

$H'$ (experimental) - $3.68 \times 10^{-5}$ g/sec-atm²

$H'$ (theoretical) - $3.97 \times 10^{-5}$ g/sec-atm²

$K_c'$ (experimental) - $5.22 \times 10^{-2}$ g-cm/sec-atm⁴

$K_c'$ (theoretical) - $4.26 \times 10^{-2}$ g-cm/sec-atm⁴

$K_D$ (experimental) - $8.64 \times 10^{-4}$ g-cm/sec

$K_D$ (theoretical) - $8.36 \times 10^{-4}$ g-cm/sec

Using the relationships outlined above and the HETP data for Podbielniak Heli-Pak No. 2917 presented previously, plots were made of the optimization factor, $S/S_m \times HETP$, as a function of boilup at various carbon-13 production rates. These curves each have minimums which represent the boilup requiring the shortest column. The optimum boilup rate as a function of carbon-13 production rate is shown in Figure 6. The average relative volatility was not significantly changed by changes in boilup rate close to the optimum.

Calculations previously reported as based on a rate of 1.0 gram carbon-13 per day were actually based on 1.0 gram carbon-13 monoxide per day production rate. By using the boilup rate indicated by the optimization study above, calculations show that a 48 millimeter ID column , 43 feet long can produce 1.0 gram carbon-13 per day; this product is carbon-13 monoxide at 90 per cent concentration with 60 per cent recovery of carbon-13 from feed carbon monoxide.

At design conditions, the 43-foot column contains 272 grams of carbon-13 as column holdup. Accumulation of this at the design rate of 1.0 gram per day would require about nine months to start up the column. At the optimum boilup of 2300 milliliters per hour this column provides 1030 theoretical stages. During the early part of the start-up period when the bottom concentration is only 10 to 20 per cent $C^{13}O$, only 284

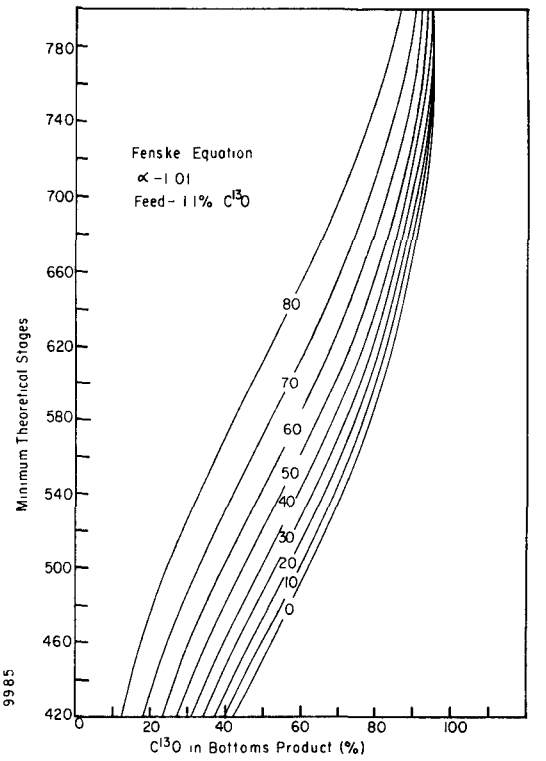


**Figure 5.** *Minimum Theoretical Stages for Separation of $C^{13}O$ From $C^{12}O$.*

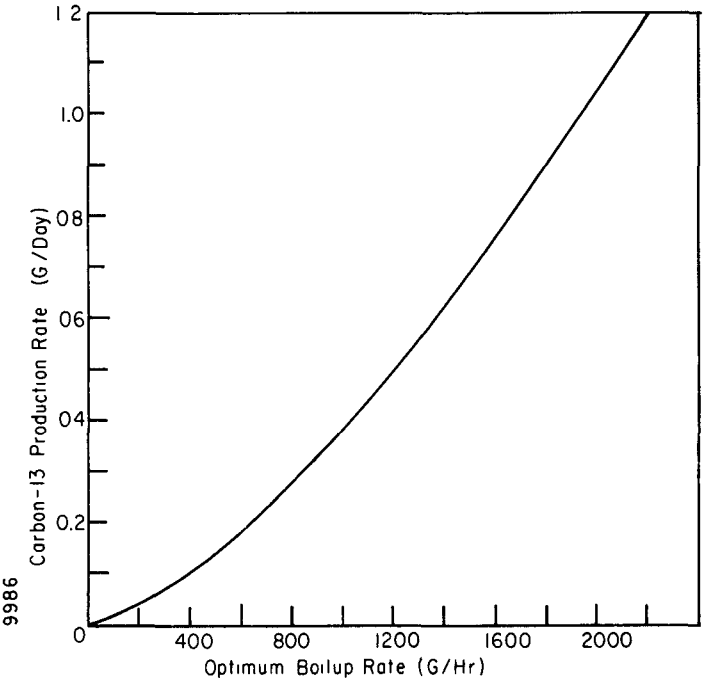


**Figure 6.** *Optimum Boilup as a Function of the Carbon-13 Production Rate Which Allows Minimum Column Length; a variation of ± 10% from the optimum boilup increases the column length less than 6%.*

theoretical stages are required at total reflux. This permits (1) boilup to be increased to the maximum rate allowable by pressure drop considerations even though total stages are reduced (HETP increases), and (2) feed rate (thus, rate of C-13 accumulation) to be increased to provide the reflux ratio appropriate for the stages available. At this stage the accumulation rate of carbon-13 can be increased to 5.70 grams per hour by increasing the boilup to 6000 milliliters per hour and reducing recovery to 20 per cent. Detailed calculations of the optimum boilups, feed rates, and carbon-13 accumulation rates are being made to guide column operation during the start-up period.

The average rate of accumulation can be increased by the above method to 3.8 grams per day of carbon-13 reducing the start-up time to 72 days. This period compares favorably with start-up times reported by others who have used tapered columns or a series of columns of progressively smaller diameters to reduce column inventory and thus reduce start-up time. Johns and London[19] used a 32 foot tapered column which required about 60 days to start up.

## Neon

Studies were made using two neon thermal diffusion columns in a two-stage cascade with an infinite reservoir at one end; a binary mixture was assumed. The 48-foot cascade will enrich neon-21 from the present intermediate stream, which has a neon-21 concentration of about three per cent. Gas will be circulated across the bottom of the cascade and neon-20 of over 99 per cent concentration will be drawn off at the top of the cascade. This will reduce the neon-20 in the bottom, leaving most of the neon-21, and will closely approximate a binary system of neon-21 and neon-22.

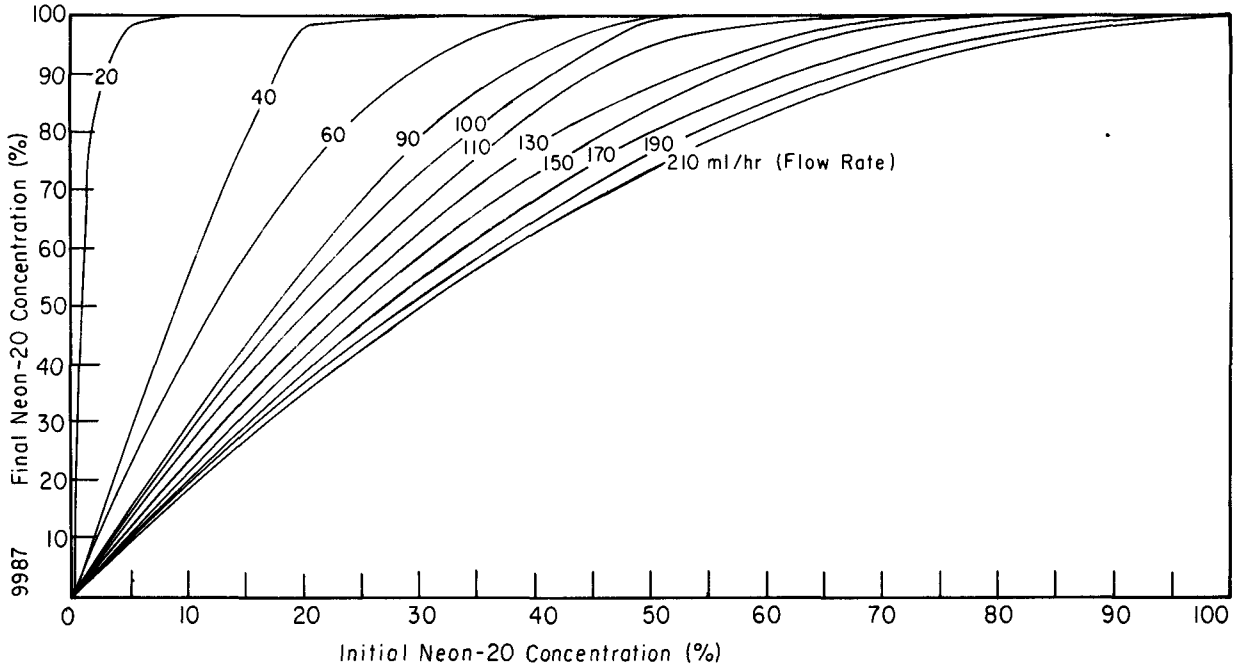


**Figure 7.** *Calculated Final Concentration of Neon-20 as a Function of Initial Concentration in Neon-22; $K_c = K_d$; Radius Ratio = 12; Temperature Ratio = 3.5.*

[19] AERE G/R661.

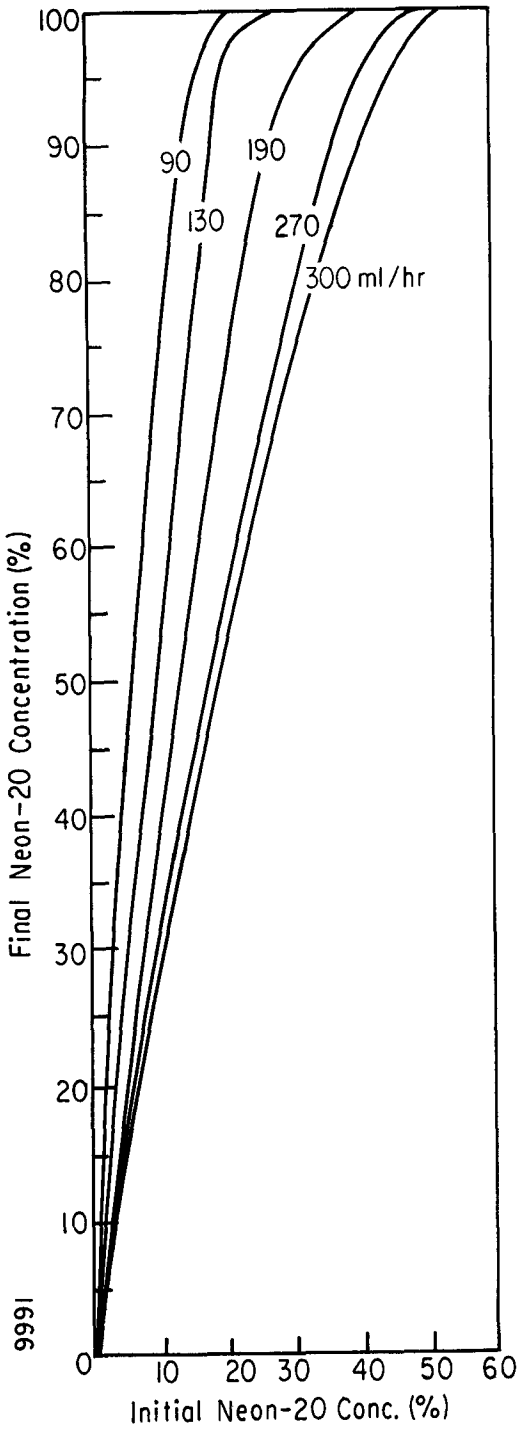


**Figure 8.** *Calculated Final Concentration of Neon-20 as a Function of Initial Concentration in Neon-22; $K_c = 10\ K_d$; 1-1 cascade of two 24-foot columns; radius ratio = 12; temperature ratio = 3.5.*

The approximate length of time and flow rate for drawing off 99 per cent neon-20 before the concentration in the reservoir at the bottom of the column would drop to a low value were determined. The value $C_I$ (reservoir, or initial concentration) was plotted as a function of $C_F$ final concentration at the top of the column) were calculated for the two cases, $K_c = K_d$ and $K_c = 10K_d$, at various product flow rates (Figures 7 and 8). The calculated time for drawing off 99 per cent neon-20 from the cascade was about 52 days. The neon-20 content in the reservoir was subsequently reduced to about 10 per cent. Similar calculations are being made for a mixture of neon-21 and neon-22. This will give the maximum time for removing neon-22 from the system. This time estimate serves only as a guide; the actual time will be determined experimentally, and the final neon-21 enrichment may have to be determined for single batches.

## Krypton

*Thermal Diffusion* A two-column, hot-wire, thermal diffusion cascaded unit with an infinite reservoir at the bottom processed natural krypton in the first step toward obtaining a final enrichment of over 90 per cent krypton-78 and -80. Batch runs were made starting with 2.7 per cent krypton-78 and -80 and a column pressure of 330 torr. The first intermediate overhead product, withdrawn at a rate of 15 milliliters per hour, started with a concentration of about 12 per cent krypton-78 and -80; this concentration decreased to about eight per cent, providing 9-10 per cent material for the next step. Withdrawal of material reduced the column pressure to 290 torr. Twenty-four liters of krypton containing nine per cent krypton-78 and -80 and eight per cent hydrogen and nitrogen have been accumulated.

| | Equilibration Time (hrs) |
|---|---|
| Theoretical | 17.5 |
| Experimental | 18.0 |
| | 24.0 |

| | Krypton-78 and Krypton-80 Concentration % | |
|---|---|---|
| | Top | Reservoir |
| | 11.50 | 2.76 |
| | 13.81 | 2.62 |
| | 14.85 | 2.61 |

To allow longer runs of 12 days on the first step, the reservoir volume was increased to 100 liters. By using this large reservoir volume, the krypton-78 and -80 reservoir concentration was not depleted significantly during equilibration as previously. Comparison of Run No. 16 equilibration performance with theory is shown below. With the original 23-liter reservoir tank krypton-78 and -80 would decrease to 2.45 per cent in the reservoir tank after 24 hours equilibration time. The time required to accumulate one liter of 90 per cent krypton-78 and -80 on a revised four-step scheme was estimated to be over one year.

*Krypton-85 Half-Life Sample* In conjunction with the work on krypton and xenon, an accurate value will be determined for the half-life of krypton-85. Accordingly, a sample containing 0.4 per cent krypton-85 will be concentrated, and the half-life will be measured calorimetrically.

Since the capsule for the gas sample will be filled to approximately 1000 psig, a capsule was designed to eliminate most of the welded joints. The bottom of the capsule will be machined from a 316 stainless steel cylinder one inch in diameter, and a high-pressure fitting will be electron beam welded into one end.

The capsule, approximately three inches long, will be disconnected from the chromatograph (in which the krypton is enriched) while immersed in liquid nitrogen to keep the sample frozen. Air permitted into the capsule during this operation will not affect the calorimetric measurements.

# ALPHA AND NEUTRON SOURCE DEVELOPMENT

*Mound Laboratory is responsible for producing alpha and neutron sources, manufactured from polonium-210 and plutonium-239, which cannot be produced by American industry at the present time. The techniques of fabricating these unusual sources are being developed and publicized.*

## Neutron Sources

Measurements were made to determine the effect of changes in temperature of the precision long counter (PLC) on the measured counting rates for neutron sources. These measurements, undertaken to explain inconsistencies in data on the growth rates of neutron sources, were made with the internal standard source and an external source. The results for the internal source agreed with a simple physical model; however, the initial results for the external source were inconclusive.

Automatic counting equipment was used for continuous measurements as the PLC was heated with a forced air heater. The counting rate changed from 531.8 cps (counts per second) to 530.5 cps for a PLC temperature increase of seven degrees. On the basis of this measurement, the counting rate for the internal source decreased about 0.035 per cent for a temperature increase of one degree Centigrade.

The fluctuation of counting rate with temperature may be explained by assuming that the source moves perpendicularly to the axis of the $BF_3$ counter due to expansion of the polyethylene holder, or moderator. The counting rate, therefore, is proportional to the inverse square of the distance of the source from the counter. Mathematically this may be expressed as

$$A = \alpha \frac{\exp(-\mu R)}{R^2}$$

and

$$\frac{d(\mu R)}{dT} = 0$$

where A is the counting rate; R is the distance between the source and the counter, $\mu$ is the attenuation coefficient; and $T$ is the temperature. Then,

$$\frac{\Delta A}{A} = -\frac{2\Delta R}{R}$$

if $\Delta R = RC(T_2 - T_1)$, where $C$ is the linear expansion coefficient and $T_1$ and $T_2$ are the initial and final temperatures, respectively, then

$$\frac{\Delta A}{A} = -2C(T_2 - T_1).$$

Since $C = 17 \times 10^{-5}$ per degree Centigrade for polyethylene,

$$\frac{\Delta A}{A} = -34 \times 10^{-5}(T_2 - T_1)$$

a 0.034 per cent decrease occurs in the counting rate for a temperature increase of one degree Centigrade.

These general results would be applicable to any moderated neutron counter where the source and counter tube(s) are within the moderator. If the moderator material, commonly polyethylene or paraffin, were constrained

in its expansion, the explanation would not be as straightforward.

Inconclusive results with the external source indicated a counting rate increase of about 0.015 per cent per degree Centigrade; however, this fluctuation has not yet been adequately explained.

*Methods of analyzing elements and compounds are being developed to support other programs at Mound Laboratory. These methods include instrumental techniques and classical wet methods.*

## Calorimetry

The most precise and accurate calorimetric determinations are currently made by comparing the bridge unbalances of a sample and a calibrating heater with a recorder; in this determination all but 25 to 100 microvolts are suppressed by resistance shunting one of the sample arms of the bridge. A potentiometer system is used to measure the power supplied to the heater, to set in the bridge current, and occasionally to measure the sensitivity of the calorimeter.[20]

An idealized bridge with shunt is shown in Figure 9. The shunt resistance $R_s$ is obtained by a decade box with six decades from 10 ohms to 10 megohms. All four arms of the bridge, with no heat in the calorimeter, have the same resistance, $R_o$. A sample (or heater) changes the sample side arms by $\Delta R$ ohms. All calorimeters have five milliamperes of bridge current except Calorimeter 60 which has two milliamperes. The bridge unbalance is taken from inside the calorimeter (below water level) by means of the input leads.

The advantage of the method is obvious; a continuous recording of the calorimeter output gives more information with less work than the sampling technique using a potentiometer-galvanometer system. The reasons for the superior precision and accuracy of the system are less apparent. First, constancy of the bridge current is less critical. In fact, it is less critical by the ratio of the total change in potential divided by the unsuppressed bridge potential; it is almost a null method. Second, there is no error resulting from the decade box if the resistance does not change between sample and heater runs. This is partly true of the potentiometer method, but in addition it must be possible to return to the same settings on the potentiometer without error

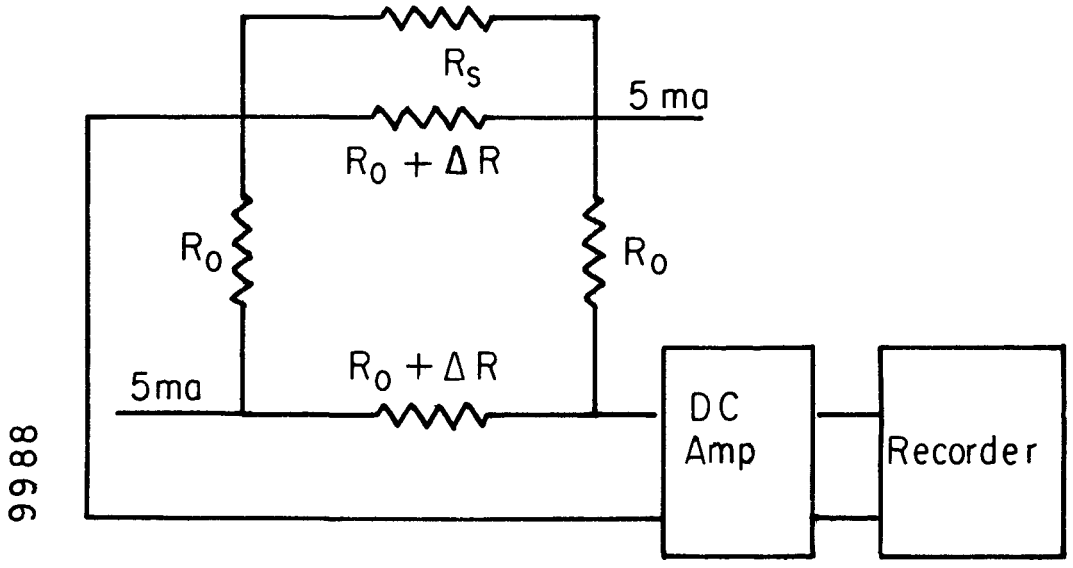


**Figure 9.** *Idealized Calorimeter Bridge With Shunt.*

[20]MLM-1144.

and also to depend on the constancy of the standard cell. Third, any thermal emf developed in the shunt circuit is reduced to the DC amplifier by the ratio $R_s/R_o$, which is usually greater than ten. With the potentiometer method there are more juntions in which thermal emf's can originate, and each one is directly in series with the bridge potential.

Sample power $W_s$ is calculated as follows:

$$W_s = W_h + \frac{D_s - D_h}{S_r} \text{ microvolts} \qquad (1)$$

where $D_s$ and $D_h$ are the displacements in chart divisions of the sample and heater equilibriums. The overall sensitivity of the system $S_r$ in divisions per microwatt is difficult to evaluate accurately. In most cases, an error of a few per cent in $S_r$ results in an insignificant error in $W_s$, However, $S_r$ can be calculated to within one per cent over the entire range of the calorimeter. The sensitivity, as measured without the shunt by the potentiometer-galvanometer system is the change in bridge potential $\Delta BP_h$ divided by the heater power, i.e.,

$$S = \frac{\Delta BP_h}{W_h} \text{ microvolts - microwatt}^{-1} \qquad (2)$$

When $S$ is plotted as a function of $W_h$, a straight line is obtained which decreases slightly with increasing $W_h$. The line can be represented as follows:

$$S = S_o(1-aW_h) \text{ microvolts - microwatts}^{-1} \qquad (3)$$

It can be shown that the sensitivity to be used in correcting for the difference between the sample and heater bridge potentials (without the shunt) is

$$S = S_o(1-2aW_h) \text{ microvolts - microwatts}^{-1} \qquad (4)$$

Equation 4 must be modified for use in Equation 1, since the shunt causes the sensitivity to decrease by a factor $F$. Also, the sensitivity of the DC amplifier and recorder must be included. This sensitivity can be expressed as $K$ chart divisions per microvolt. Thus,

$$S_r = FKS_o(1-2aW_h) \text{ chart divisions - microwatt}^{-1} \qquad (5)$$

The factor $F$ can be expressed in terms of the ratio of the shunt resistance to the zero bridge resistance $R_s/R_o$ by the following equations:

$$F = \frac{2(f^2+1)}{f^2(f+1)^2} \qquad (6)$$

$$f_s = \frac{R_s}{R_o} = \frac{f}{f^2-1} \qquad (7)$$

$$f = 1 + \frac{\Delta R}{R_o} \qquad (8)$$

Numerical values for $f$ can be assumed, and the corresponding values for $F$ and $f_s$ can be calculated by Equations 6 and 7. A graph which is valid for all calorimeters can then be plotted of $F$ as a function of $f_s$.

Table 6 gives selected values from this graph. The values of $f$ in Table 6 go from 1.005 to 1.060 in increments of 0.005. An $f$ of 1.060 corresponds to an average temperature rise in the bridge of 11.1°C when the bridge is wound of 99 alloy nickel wire. The temperature rise in the central section will be about twice the average, or 22°C. This is as high as the average calorimeter should be taken in a water bath at room temperature.

**Table 6**

**SENSITIVITY CORRECTION FACTORS DUE TO SHUNTING ONE ARM OF A RESISTANCE BRIDGE CALORIMETER**

| $(R_s/R_o)$[a] | (F)[b] | $(R_s/R_o)$ | (F) |
|---|---|---|---|
| 100.25 | 0.9901 | 14.531 | 0.9338 |
| 50.25 | 0.9803 | 12.745 | 0.9249 |
| 33.58 | 0.9707 | 11.356 | 0.9162 |
| 25.25 | 0.9613 | 10.244 | 0.9076 |
| 20.25 | 0.9520 | 9.334 | 0.8991 |
| 16.913 | 0.9428 | 8.576 | 0.8908 |

[a] Ratio of shunt resistance to zero bridge resistance.

[b] To be multiplied by sensitivity without shunt.

**Beryllium by Gamma Activation Analysis**

The irradiation and counting systems used in the gamma activation analysis of beryllium have been modified to incorporate four Texlium[21] helium-3 filled neutron counting tubes in place of the indium foil formerly used.[22]

The tubes, made of stainless steel 10.5 inches long by 0.5 inch in diameter, are filled to six atmospheres pressure with high purity helium-3. Helium-3 has a neutron cross section of 5200 barns for the *(n,p)* reaction. The energetic proton released in the *(n,p)* reaction causes gas ionization at 850 volts, whereas gamma radiation will not produce ionization until 1050 volts. This difference allows complete gamma discrimination on the operating plateau of 950 to 1000 volts.

In the arrangement now used for analyses (Figure 10), the antimony-124 is placed permanently in the center of the paraffin-filled drum. The four Texlium tubes are equally spaced around the source 2.5 inches from center. The paraffin drum is shielded with eight inches of lead with a two-inch opening on the top, through which the beryllium sample in the Lucite irradiation chamber is lowered over the gamma source. The geometry is held constant by a 1.5-inch ID quartz guide tube.

Beryllium samples are weighed and encapsulated in polyethylene vials, one inch by 0.5 inch. They are placed in the Lucite irradiation chamber and lowered over the source; then the guide hole is covered with a two-inch lead brick. The sample is neutron counted for five minutes and removed, and a standard is counted for five minutes. This is repeated three times or until a gross count of 500,000 counts is accumulated.

[21] Texas Nuclear Corp., Austin, Texas.

[22] MLM-1155; MLM-1160.

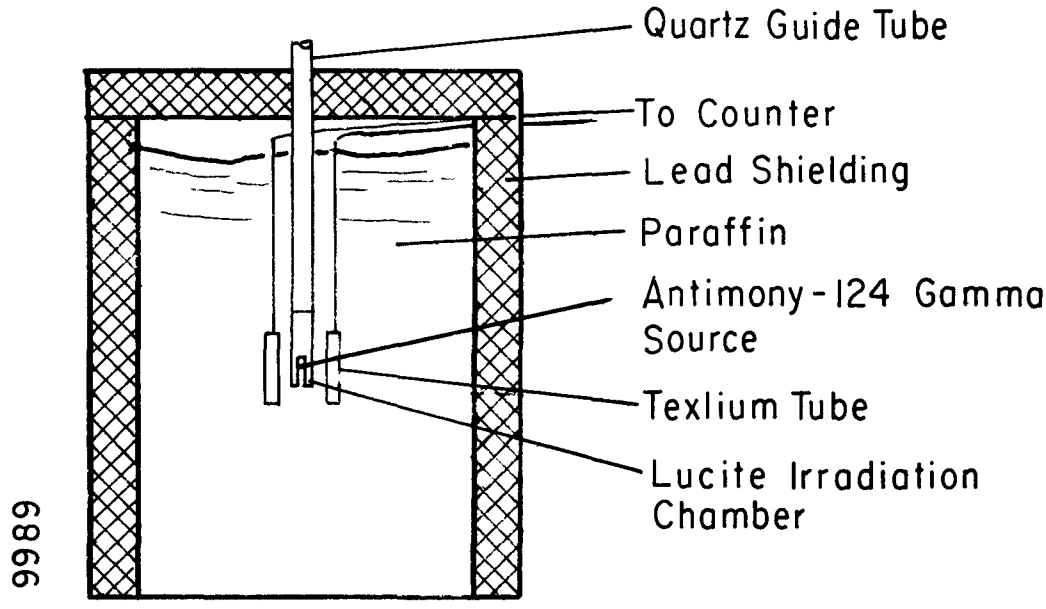


**Figure 10.** *Apparatus for Gamma Activation Analysis of Beryllium*

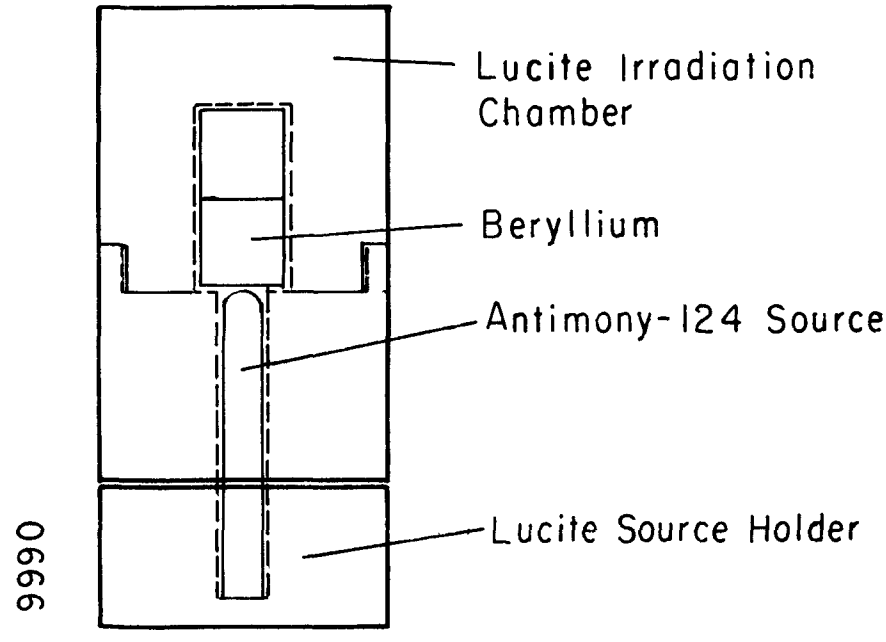


**Figure 11.** *Apparatus for Gamma Activation Analysis of a Beryllium Powder Sample*

With powdered beryllium, the count rate is not directly proportional to the weight of beryllium in the sample due to the placement of the neutron detectors. In this arrangement (Figure 11), the beryllium absorbs the gamma flux penetrating to the top of the sample; thus, the more sample in the polyethylene vial, the greater the absorbency. Therefore, the average flux is given by:

$$\ln f = \frac{C_1}{W_s} \qquad (1)$$

where

$f$ = average gamma flux

$C_1$ = gamma flux produced by source, which is constant

$W_s$ = weight of sample

The neutron count rate is given by:

$$d/min = \delta f n (1 - e^{-\lambda t}) \qquad (2)$$

where

$d/min$ = disintegrations per minute

$\delta$ = neutron cross section = constant $C_2$

$f$ = average gamma flux

$n = \frac{\text{Weight beryllium}}{\text{atomic weight}} \times 6.02 \times 10^{23} = W_{Be} \times \text{constant } C_3$

$(1 - e^{-\lambda t})$ = decay factor = 1

If the constants are combined and the equation is converted to log form, Equation (2) becomes

$$\ln d/min = c \ln f \ln W_{Be} \qquad (3)$$

The final equation is derived by combining equations (1) and (3):

$$\ln d/min = C \frac{\ln W_{Be}}{W_s} \qquad (4)$$

For analysis, the constant in Equation (4) is evaluated using beryllium standards. The unknown weight of beryllium is determined using the count rate produced from the sample and the constant.

The Texlium tubes have increased the counting efficiency by a factor of 500. A 0.05-curie antimony-124 gamma source is now used instead of the original three-curie source. This smaller source makes the procedure less hazardous while maintaining the high neutron count rate necessary for rapid and accurate analysis. With the new arrangement a two-gram beryllium sample has a count rate of 41,000 cpm. Samples have been analyzed with the new system using a 99.98 per cent pure beryllium standard, and the results were compared to those from the cupferron method. The first lot of six tests gave an average 98.36 per cent beryllium by gamma activation analysis; the deviation was ± 0.06 per cent. In comparison, the cupferron analysis yielded an average 98.39 per cent for four samples. The second lot of four samples yielded 98.69 per cent beryllium with a deviation of ± 0.14 per cent as compared to 98.62 per cent for beryllium by the cupferron method.